DMS emissions from the Arctic marginal ice zone

Martí Galí, Martine Lizotte, David Kieber, Achim Randelhoff, Rachel Hussherr, Lei Xue, Julie Dinasquet, Marcel Babin, Eric Rehm, Maurice Levasseur

ELEMENTA
Science of the Anthropocene

Galí, M, et al. 2021. DMS emissions from the Arctic marginal ice zone. *Elem Sci Anth*, 9: 1. DOI: https://doi.org/10.1525/elementa.2020.00113

RESEARCH ARTICLE

DMS emissions from the Arctic marginal ice zone

Martí Galí[1,2,3,*], Martine Lizotte[1,2], David J. Kieber[4], Achim Randelhoff[1,2], Rachel Hussherr[1,2], Lei Xue[4], Julie Dinasquet[5,6], Marcel Babin[1,2], Eric Rehm[1,2], and Maurice Levasseur[1,2]

Phytoplankton blooms in the Arctic marginal ice zone (MIZ) can be prolific dimethylsulfide (DMS) producers, thereby influencing regional aerosol formation and cloud radiative forcing. Here we describe the distribution of DMS and its precursor dimethylsulfoniopropionate (DMSP) across the Baffin Bay receding ice edge in early summer 2016. Overall, DMS and total DMSP ($DMSP_t$) increased towards warmer waters of Atlantic origin concurrently with more advanced ice-melt and bloom stages. Relatively high DMS and $DMSP_t$ (medians of 6.3 and 70 nM, respectively) were observed in the surface layer (0–9 m depth), and very high values (reaching 74 and 524 nM, respectively) at the subsurface biomass maximum (15–30 m depth). Microscopic and pigment analyses indicated that subsurface DMS and $DMSP_t$ peaks were associated with *Phaeocystis pouchetii*, which bloomed in Atlantic-influenced waters and reached unprecedented biomass levels in Baffin Bay. In surface waters, DMS concentrations and DMS:$DMSP_t$ ratios were higher in the MIZ (medians of 12 nM and 0.15, respectively) than in fully ice-covered or ice-free conditions, potentially associated with enhanced phytoplanktonic DMSP release and bacterial DMSP cleavage (high *dddP*:*dmdA* gene ratios). Mean sea–air DMS fluxes (μmol m^{-2} d^{-1}) increased from 0.3 in ice-covered waters to 10 in open waters (maximum of 26) owing to concurrent trends in near-surface DMS concentrations and physical drivers of gas exchange. Using remotely sensed sea-ice coverage and a compilation of sea–air DMS flux data, we estimated that the pan-Arctic DMS emission from the MIZ ($E_{DMS,\ MIZ}$) was 5–13 Gg S yr^{-1}. North of 80°N, $E_{DMS,\ MIZ}$ might have increased by around 10 ± 4% yr^{-1} between 2003 and 2014, likely exceeding open-water emissions in June and July. We conclude that $E_{DMS,\ MIZ}$ must be taken into account to evaluate plankton-climate feedbacks in the Arctic.

Keywords: Dimethylsulfide, Dimethylsulfoniopropionate, Arctic, Marginal ice zone, Microbial plankton, *Phaeocystis pouchetii*

1. Introduction

The shrinking and thinning of Arctic sea ice are among the most striking consequences of anthropogenic global warming (Arctic Monitoring & Assessment Programme [AMAP], 2017; Intergovernmental Panel on Climate Change [IPCC], 2019). Model projections indicate that the Arctic could become entirely ice free in summer by 2040–2050 (Thackeray and Hall, 2019). In this new regime, devoid of multiyear ice, the belt of retreating sea ice known as the marginal ice zone (MIZ) will move every year from its southernmost extent in late winter to its northernmost extent prior to complete melt in late summer. Therefore, biogeochemical processes occurring within the MIZ, including the emission of biogenic gases and particles to the atmosphere, have the potential to reshape marine ecosystems and geosystems across the entire Arctic Ocean.

The MIZ is an ephemeral environment, in this study operationally defined as the zone where the sea-ice cover decreases from nearly total (>85%) to nearly absent (<15%) before permanent ice opening in spring and summer. Several tens or a few hundred kilometers wide (Strong, 2012; Strong and Rigor, 2013) and with a duration of days to weeks (Randelhoff et al., 2019), the MIZ hosts intense exchanges of freshwater, heat and momentum between the ocean and the atmosphere (McPhee, 2008). From a biogeochemical standpoint, the MIZ period marks the transition between two major blooms of microalgae in the Arctic. Prior to the melt season, biological activity generally concentrates in the bottom layer of the sea ice, where sympagic algae grow massively as soon as sufficient light penetrates through the ice or snow surface (Leu et

[1] Takuvik International Research Laboratory, Laval University (Canada), CNRS, France
[2] Département de biologie et Québec-Océan, Université Laval, Québec City, QC, Canada
[3] Barcelona Supercomputing Center (BSC)
[4] Department of Chemistry, College of Environmental Science and Forestry, State University of New York, Syracuse, NY, USA
[5] Marine Biology Research Division, Scripps Institution of Oceanography, La Jolla, CA, USA
[6] Sorbonne Université, Laboratoire d'Océanographie Microbienne, Banyuls-sur-Mer, France

* Corresponding author:
Email: marti.gali.tapias@gmail.com

al., 2015). When sufficient sunlight crosses the sea ice or the free ocean surface, phytoplankton can also bloom in the water column, taking advantage of nutrient stocks replenished over the winter and stable stratification caused by ice melt. These pulses of sympagic and pelagic algal growth, largely dominated by diatom species, account for a major portion of annual primary production in polar waters (Perrette et al., 2011; Wassmann and Reigstad, 2011; Renaut et al., 2018) and result in the emission of a wide diversity of biogenic particles and gases to the atmosphere (Levasseur, 2013; Gabric et al., 2018; Abbatt et al., 2019).

Biogenic emissions play an important role in the Arctic climate in late spring and summer, when biological activity is maximal and the atmosphere is depleted of aerosols (both natural and anthropogenic; Abbatt et al., 2019). The low aerosol baseline, caused by limited transport from lower latitudes and efficient scavenging (Heintzenberg et al., 2015; Croft et al., 2016), favors secondary aerosol formation from local gaseous emissions (Leaitch et al., 2013; Collins et al., 2017). The gas dimethylsulfide (DMS) is, quantitatively, the main volatile organic compound emitted by the activity of marine and sea-ice microbes (Simó, 2011; Carpenter et al., 2012). In the clean Arctic atmosphere, DMS oxidation end-products (mostly, sulfuric and methanesulfonic acids) readily form new aerosol particles that scatter sunlight (Dawson et al., 2012; Leaitch et al., 2013; Hodshire et al., 2019; Veres et al., 2020; Brean et al., 2021). Moreover, DMS derivatives contribute to the condensational growth of aerosols into cloud condensation nuclei (CCN; Ghahremaninezhad et al., 2019), altering the balance between cloud shortwave forcing (increasing cloud albedo) and longwave forcing (increasing heat retention) (Andreae and Rosenfeld, 2008; Carslaw et al., 2013; Mahmood et al., 2019). In aerosol-depleted areas and over the pack ice, this radiative balance is particularly sensitive to local CCN sources (Mauritsen et al., 2011). Thus, ongoing changes in DMS emission patterns and their underlying drivers (Six et al., 2013; Galí et al., 2019) can influence the ensemble of climate feedbacks, known as Arctic amplification, that cause the Arctic to warm faster than the global average (Serreze and Barry, 2011). In turn, changes in atmospheric radiative transfer and ice dynamics can modulate phytoplankton productivity, potentially establishing a feedback mechanism (Charlson et al., 1987) that has yet to be verified (Quinn and Bates, 2011).

DMS emission (EDMS) in the Arctic originates from both surface seawater and ice environments such as the ice bottom (Galindo et al., 2014) and saline melt ponds (Gourdal et al., 2018; Park et al., 2019). Current estimates obtained with different approaches indicate that ice-free waters largely dominate EDMS regionally at the pan-Arctic level (Lana et al., 2011; Galí et al., 2019; Hayashida et al., 2020). Yet, DMS has an atmospheric lifetime of a few days, at most, which limits atmospheric transport and magnifies the effects of local DMS sources on aerosols in conjunction with local meteorological conditions. Recent studies highlighted the broad variability and patchiness in tropospheric DMS concentrations (Mungall et al., 2016; Ghahremaninezhad et al., 2019), and also the episodic nature of new particle formation events (Collins et al., 2017; Dall'Osto et al., 2017; Heintzenberg et al., 2017). These findings stress the need to better understand and quantify DMS emissions from ephemeral environments such as the MIZ that can produce intense but short-lived emission events.

The emission of DMS from seawater results from a complex network of biotic and abiotic processes (Simó, 2001). The primary precursor of DMS is dimethylsulfoniopropionate (DMSP), a compound synthesized mainly by marine algae (Stefels et al., 2007) and also by some bacteria (Curson et al., 2017). In phytoplankton, DMSP serves different physiological functions such as osmoregulation, antioxidation or cryoprotection (Stefels et al., 2007), and its intracellular concentrations vary widely across taxonomic groups, with most high DMSP producers found among the haptophytes and dinoflagellates (Keller, 1989; McParland and Levine, 2019). Conversion of DMSP to DMS proceeds mostly through the enzymatic cleavage by algal (Alcolombri et al., 2015) and bacterial (Curson et al., 2011) DMSP-lyase enzymes. The cleavage pathway typically accounts for <30% of the microbial DMSP consumption (Kiene and Linn, 2000; Galí and Simó, 2015), and the remainder is transferred to bacteria and protists and diverted away from DMS production. However, the efficiency of the conversion of DMSP to DMS can vary widely in response to food-web processes, such as grazing (Simó et al., 2018), bacterial metabolism (Kiene et al., 2000), and environmental stressors, such as nutrient limitation (Sunda et al., 2007), high irradiance (Galí et al., 2013), and ocean acidification (Bénard et al., 2021). In the upper mixed layer of the ocean, dissolved DMS is readily transformed to dissolved non-volatile sulfur species by DMS-consuming bacteria (Kiene and Bates, 1990; del Valle et al., 2009; Lidbury et al., 2016) and photolysis (Kieber et al., 1996; Galí et al., 2016). In consequence, typically less than 15% of the DMS produced in the upper mixed layer is vented to the atmosphere in ice-free waters (Galí and Simó, 2015).

The multiple biogeochemical pathways that mediate between DMSP synthesis and DMS emission generally tend to buffer DMS concentrations in open ocean settings (Galí and Simó, 2015), where sea-surface DMS concentrations above 10 nM are rare (Lana et al., 2011). In the MIZ, however, seawater DMS concentrations and sea–air DMS fluxes (F_{DMS}) can greatly increase when some factors co-occur, namely: the formation of massive phytoplankton blooms (Perrette et al., 2011; Arrigo et al., 2014; Renaut et al., 2018) depending on the type of ice edge (multi-year versus first-year sea ice; Lizotte et al., 2020); the presence of high DMSP and DMS producers (Levasseur, 2013); the enhancement of DMS production by food-web interactions or physiological stress (Matrai et al., 1995; Sunda et al., 2007; Galí et al., 2013); and weak biological DMS removal during early bloom stages (del Valle et al., 2009). Among these factors, blooms of the colony-forming haptophyte *Phaeocystis* are thought to play a prominent role. This genus has an intracellular DMSP content of about 5%–10% of cell carbon, roughly one order of magnitude higher than diatoms and, unlike diatoms, displays high

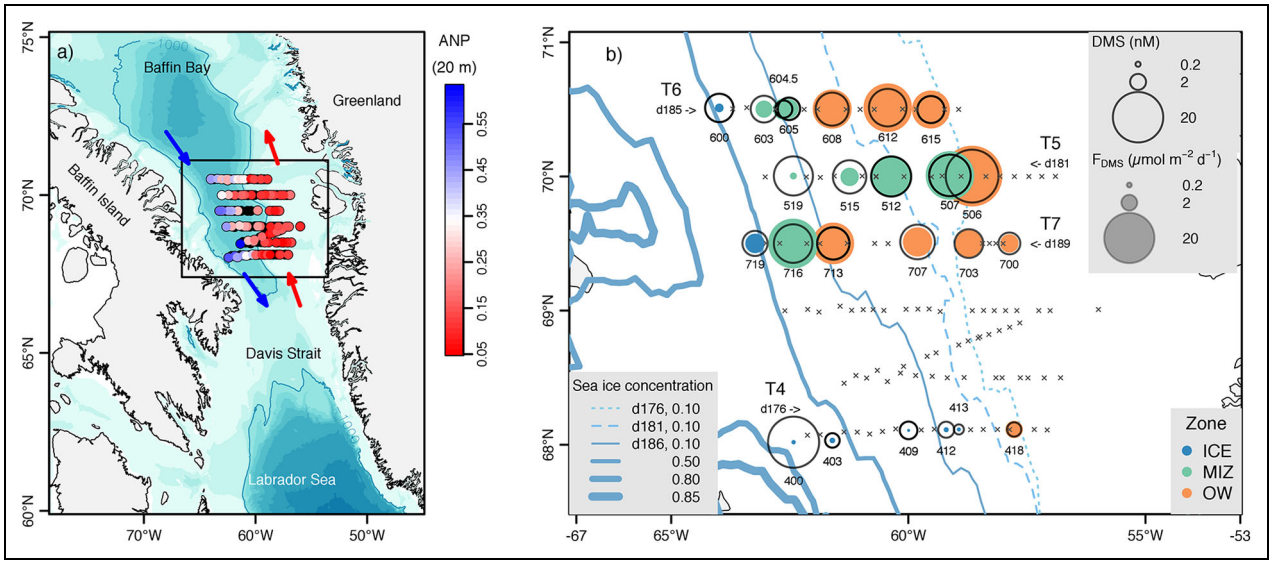

Figure 1. Maps of the study area and sea-surface DMS concentrations and fluxes (F_{DMS}). (a) Bathymetric map of southern Baffin Bay, Davis Strait and northern Labrador Sea. Dots show the grid of Green Edge cruise stations, colored according to the "Arctic N-P relationship" (ANP) at 20 m, which distinguishes waters of Arctic (blue) and Atlantic (red) origin, whose approximate circulation is shown by arrows; (b) close-up of the study area. The size of empty and filled circles indicates the magnitude of sea-surface DMS concentrations and sea–air DMS fluxes, respectively, and the color of filled circles indicates whether a station is classified as ICE, MIZ, or OW (**Table 1**). Contours of satellite-retrieved sea-ice fractional coverage are shown in different textures and shades of blue for different periods of 5 days of the year: d176–d180 (0.10 contour), d181–d185 (0.10 contour), and d186–d190 (0.10, 0.50, 0.80, and 0.85 contours). Sampled stations and the start dates of sampled transects (Julian day, d) are also indicated. Stations not sampled for sulfur compounds are marked with crosses. DOI: https://doi.org/10.1525/elementa.2020.00113.f1

DMSP-lyase activity (Sheehan and Petrou, 2019; Stefels et al., 2007). These factors, together with the global distribution of bloom-forming *Phaeocystis* species, make *Phaeocystis* blooms a major source of atmospheric DMS globally (Schoemann et al., 2005; Wang et al., 2015).

In this article we describe spatial DMS and DMSP concentration patterns across a receding first-year ice edge in Baffin Bay, seeking to disentangle the role of Pacific-derived Arctic water masses and Atlantic water masses, meltwater stratification, and phytoplankton bloom progression, with particular attention to *Phaeocystis pouchetii*. Finally, we compare our findings to a compilation of in situ studies, and upscale in situ observations using remote sensing to provide pan-Arctic estimates of DMS emission from the MIZ ($E_{DMS,\ MIZ}$) between 2003 and 2016.

2. Methods

2.1. Hydrographic data

The Green Edge expedition sampled seven transects across the ice edge in southern Baffin Bay, north of the Davis Strait (approximately at 70°N and 60°W) aboard the CCGS *Amundsen* research icebreaker. Here we report measurements from four East–West transects, named T4, T5, T6 and T7, sampled during the second leg of the cruise between June 24 and July 10, 2016 (**Figure 1**). At each station along a given transect, vertical profiles of water column properties were measured down to at least 300 m using a sampling rosette with attached Seabird SBE-911 plus conductivity-temperature-depth (CTD) sensors, a Seapoint chlorophyll fluorometer, and a WetLabs C-Star transmissometer (0.25-m pathlength). The CTD data were processed according to standard Amundsen Science Team procedures (P Guillot, personal communication). Transmissometer profiles were used to calculate the beam attenuation coefficient at 650 nm due to particles, c_p (m^{-1}), following standard procedures (Loisel and Morel, 1998). Particulate organic carbon (POC; units of mg m^{-3}) was estimated from c_p using a conversion factor of 500 mg POC m^{-2} (Cetinić et al., 2012, and references therein). Water samples were collected at several depths using Niskin bottles mounted on the CTD rosette for the determination of dimethylated sulfur compounds (Section 2.4), phytoplankton pigments and abundance (Section 2.6), bacterial abundance and sulfur metabolism (Section 2.7), and inorganic nutrients (nitrate, nitrite, phosphate, and silicate; Koroleff and Hansen, 1999; see details in Randelhoff et al., 2019).

2.2. Satellite sea-ice concentration data sets

Sea-ice fractional coverage was retrieved from microwave satellite sensors, and will be referred to as sea-ice concentration (SIC) hereafter, following the conventional name of the remote sensing products. Daily SIC images from the Advanced Microwave Scanning Radiometer 2 (AMSR2) on a 3.125-km grid (Spreen et al., 2008) were downloaded from ttp://www.iup.uni-bremen.de:8084/amsr2data/asi_daygrid_swath/n3125/ and used to describe ice dynamics over the entire melt season in the Green Edge study area (**Figure 1**). From this dataset, a SIC time series for each station was extracted from the closest satellite pixel.

Table 1. Physical and biogeochemical characteristics of the stations across the ice edge, classified according to the open water days (OWD) metric. DOI: https://doi.org/10.1525/elementa.2020.00113.t1

	Ice-Cover Category		
Characteristic	**ICE**	**MIZ**	**OW**
Descriptors of the stations			
OWD thresholds (d)	OWD < –3	–3 ≤ OWD ≤ 3	OWD > 3
Mean observed OWD	–12	0	13
SIC thresholds (%) (days –2, –1, 0)[a]	SIC > 85	85 ≥ SIC ≥ 15	SIC < 15
Mean observed SIC (%) (days –2, –1, 0)[a]	94, 93, 90	52, 45, 15	0, 1, 0
Arctic-domain stations	400, 403, 406, 600, 719	519, 603, 604.5, 605, 716	608, 700, 703, 707, 713
Atlantic-domain stations	409, 412, 413	507, 512, 515	418, 506, 612, 615
Total number of stations	8	8	9
Descriptors of the water column physics and biogeochemistry: mean (min–max)			
MLD0.03 (m)[b]	6 (2–22)	3 (1–5)	7 (1–15)
h_{BD} (m)[c]	20 (15–32)	15 (11–17)	18 (12–31)
Isolume 0.415 (m)	26 (11–41)	35 (21–47)	42 (29–60)
Nitracline (m)	1 (0–7)	4 (0–15)	21 (1–43)
SBM (m)[d]	8 (3–21)	12 (7–16)	24 (16–31)

[a] Satellite-retrieved sea-ice concentration (SIC); (days –2, –1, 0) refers to the 3-day period ending on the sampling day.

[b] Shallowest mixed layer depth where sigma-t exceeded by 0.03 kg m^{-3} the value at 1 m.

[c] Equivalent mixed layer depth (as defined by Randelhoff et al., 2017).

[d] Subsurface biomass maximum.

An additional SIC dataset for the entire Arctic between 2003 and 2016 was downloaded from the National Snow and Ice Data Center (http://nsidc.org), and consisted of images obtained by the Special Sensor Microwave/Imager (2003–2007) and the Special Sensor Microwave Imager/Sounder (2008–2016). Daily SIC images at 25-km resolution were re-projected onto a 4.64-km sinusoidal grid to better match ocean color remote sensing products, and then bin-averaged into 6 × 6 macropixels (27.84 km) and 8-day periods. This dataset was used to compute pan-Arctic estimates of $E_{DMS,\ MIZ}$ (Section 2.9) in a format that was directly comparable to previous satellite-based estimates of E_{DMS} from open waters (Galí et al., 2019).

2.3. Irradiance

Downwelling photosynthetically active radiation (PAR) immediately above the sea surface (PAR0+) was estimated with the Santa Barbara DISORT Atmospheric Radiative Transfer (SBDART) model (Ricchiazzi et al., 1998) using precomputed look-up tables (Laliberté et al., 2016). Hourly SBDART time series showed good agreement with in situ data recorded on the ship's meteorological tower (Kipp and Zonen PAR Lite; sampling frequency 1 min^{-1}), with $R^2 = 0.88$ and mean bias = –6%. Measurements taken on the ship were deemed not representative of the daily mean PAR0+ at any fixed station because they reflected rapid variations in ice albedo and fog conditions as the CCGS *Amundsen* traversed back and forth across the MIZ. Thus, the mean irradiance during the 24-h prior to sampling at each station was computed from the hourly SBDART output.

Downwelling PAR was measured in the water column down to 100 m using a Compact Optical Profiling System (C-OPS, Biospherical Instruments Inc., San Diego, CA). Underwater measurements were referenced to simultaneous above-surface measurements to calculate the vertical PAR transmittance profile for a given C-OPS cast. To correct for the effect of variable ice cover, the mean PAR transmittance profile at each station was computed as the SIC-weighted average of the closest ice-free and ice-covered C-OPS casts. To obtain the mean daily PAR profile, the mean transmittance profile was multiplied by the mean daily PAR0+ (see details about the measurements and calculations in Randelhoff et al. 2019).

2.4. DMS and DMSP sampling and analysis

DMS and DMSP samples were collected during the morning CTD cast at 8 AM local time from 5 or 6 depths between the surface and 100 m; additional samples were taken occasionally from the CTD casts performed around noon. At several intermediate hydrographic stations, located between full stations, samples were collected only from the surface (1 m) and the subsurface chlorophyll maximum (SCM). The SCM depth was estimated from fluorescence depth profiles. A total of 25 stations (**Tables 1** and S1) and 35 CTD casts were sampled.

Samples for DMS analysis were collected into 120-mL precleaned borosilicate vials leaving no head space, allowing some overflow and taking care to avoid bubbling. The vials were filled using a precleaned silicone tube connected to the Niskin bottle spigot, fitted with a 5-µm Nitex mesh at its tip to gently screen out large phytoplankton cells and colonies (Kinsey et al., 2016). Occasionally, additional vials were filled using a 100-µm mesh Nylon screen to test for DMS measurement artifacts associated with *Phaeocystis* cell breakage upon filtration. DMS samples were stored in the dark at 4°C and processed within 2 h of collection.

For DMS analysis, 10–20 mL were withdrawn from the vial, spiked with a DMS-d_6 internal standard (4.5 nM final concentration), sparged with ultra high purity helium for 5 min and trapped in a glass tube filled with Tenax-TA (kept below −10°C) using a custom-made purge-and-trap device (Gourdal et al., 2018). Trapped DMS was injected into a gas chromatograph-mass spectrometer (GC-MS; GC: Agilent 7890A; MS: Agilent 5975C) for quantification. The GC-MS was calibrated at the beginning of each transect by injections of DMS-d_3 and DMS-d_6 at 4–6 concentrations ranging between 0.5 and 45 nM, and a single calibration curve was used for the whole dataset (R^2 of the log-log linear calibration > 0.99). The peak areas of endogenous DMS and internal standards, determined with the MassHunter software, were converted to concentrations after correcting for blank signals and internal standards. No analytical replicates were analyzed for the majority of the samples. The mean propagated uncertainty of DMS measurements was estimated at 10%, which includes the replication uncertainty estimated from duplicate analyses (n = 16) and the calibration uncertainty. In addition, prefiltration tests suggested that DMS was 19% higher on average (n = 19) in samples filtered through a 100-µm mesh, compared to their 5-µm-filtered counterparts. Although this test was statistically inconclusive, it indicates the importance of sample pre-screening in the presence of *Phaeocystis* sp. (del Valle et al., 2009). Further details regarding the analysis of DMS are provided in the Supplemental Materials (Text S1).

Samples for DMSP analysis were collected in triplicate and included a set of unfiltered samples for total DMSP ($DMSP_t$) and a second set of filtered samples for dissolved DMSP ($DMSP_d$). This sampling plan enabled the calculation of particulate DMSP ($DMSP_p$) as $DMSP_t - DMSP_d$. Unfiltered seawater samples were collected into 20-mL pre-cleaned borosilicate scintillation vials screw-capped with a solid cap containing a Teflon-lined silicone insert. Samples were microwaved with the cap loosened, then bubbled with purified air to remove DMS, acidified with hydrochloric acid, and stored in the dark at room temperature (Kinsey and Kieber, 2016). Filtered samples were obtained by the small volume, gravity drip filtration method (Kiene and Slezak, 2006) using prebaked (550°C, 8 h) 25-mm diameter glass fiber filters (Whatman GF/F); samples were bubbled with purified air for several minutes to remove DMS followed by addition of hydrochloric acid and storage at room temperature in the dark.

Processed DMSP samples were analyzed at Laval University (UL, Québec City) and at the State University of New York, College of Environmental Science and Forestry (SUNY-ESF, Syracuse, NY) within 30 months of collection. Storage tests confirmed the good preservation of samples (>95% recovery), and excellent agreement between laboratories was found (mean difference of 1.2 ± 10%). At both laboratories, DMSP was analyzed as DMS after stoichiometric base (NaOH) cleavage. At UL, the evolved DMS was analyzed in a GC-MS (GC: Agilent Intuvo 9000; MS: Agilent 5977B), and peak areas determined with the MassHunter software were converted to concentration against a 7-point calibration of a diluted DMSP standard solution (R^2 > 0.99; Lizotte et al., 2020). At SUNY-ESF, DMSP was quantified following the procedure outlined in Kinsey and Kieber (2016) on a Shimadzu GC-14A with flame photometric detector. Further details on DMSP analysis are provided in Text S2.

2.5. Sea–air DMS flux (F_{DMS}) calculation

We estimated F_{DMS} (µmol m^{-2} d^{-1}) as the product of the sea–air gas transfer coefficient (K), the DMS gradient across the sea–air interface, and the ice-free water fraction (1 − SIC):

$$F_{\mathrm{DMS}} = K \cdot (\mathrm{DMS}_w - \mathrm{DMS}_a) \cdot (1 - \mathrm{SIC}). \qquad (1)$$

K was computed using the wind speed–based gas exchange parameterization of Woolf (1997) and Woolf (2005), taking into account air- and water-side resistance ($1/K = 1/k_a + 1/k_w$) and the effects of SST and salinity on DMS diffusivity and solubility, and assuming $DMS_a = DMS_w/253$ based on field measurements (Land et al., 2014). Wind speed measurements were acquired at 1 min^{-1} frequency by the anemometer installed 16 m above sea level on the ship's meteorological tower (Burgers et al., 2017), and converted to 10-m wind speeds according to a standard wind profile for neutral atmospheric stability (Hsu et al., 1994). At each station we calculated F_{DMS} using one single value for DMS_w and SST and the 1 min^{-1} time series of wind speed during the 24 h prior to sampling, and then calculated the daily mean F_{DMS}. The reader is referred to Galí et al. (2019) for further details on gas exchange calculations.

2.6. Phytoplankton pigments, abundance, carbon pools, and DMSP-biomass

Samples for phytoplankton pigment analyses were collected from Niskin bottles on the CTD rosette. Up to 2.7 L of seawater were filtered on Whatman GF/F filters to collect phytoplankton cells, and the filters contained in cryotubes were stored in liquid nitrogen until analysis. Back on land, filters were soaked in 100% methanol, disrupted by sonication, and the resulting solution of extracted pigments was clarified by filtration (GF/F) and analyzed using High Performance Liquid Chromatography (HPLC) on an Agilent Technologies HPLC 1200 system equipped with a diode array detector (Ras et al., 2008). Based on multivariate analyses (see Section 2.8), we selected the following pigments as predictors of dimethylated sulfur compounds: total chlorophyll *a* (TChl *a*; Chl

a plus allomers and epimers), chlorophyll *b* (Chl *b*), chlorophyll *c2* (Chl *c2*; in practice, Chl *c1*+*c2*), chlorophyll *c3* (Chl *c3*), fucoxanthin (Fuco), 19′-hexanoyloxyfucoxanthin (Hex-fuco), 19′-butanoyloxyfucoxanthin (But-fuco), 19′-butanoyloxyfucoxanthin-like (But-fuco-like), peridinin (Peri), prasinoxanthin (Pras), β-carotene (in practice, α + β-carotene; Ras et al., 2008), diadinoxanthin + diatoxanthin (DD), violaxanthin + antheraxanthin + zeaxanthin (VAZ) and pheophorbide *a* (Pheo *a*). Pigments were grouped as either chlorophylls, photosynthetic (light-harvesting) carotenoids (PSC), photoprotective carotenoids (PPC) or degradation products (**Table 2**) and used as physiological and taxonomic indicators.

At nine (of 25) stations, samples for identification and counting of micro- and nanophytoplankton were taken at the surface and at the depth of the fluorescence maximum, preserved in Lugol's solution and kept at 4°C. Cells were counted under an inverted microscope after sedimentation of 25–50 mL following standard procedures. In addition to traditional microscopy, an Imaging FlowCytobot (IFCB; Olson and Sosik, 2007) was used to take pictures of phytoplankton and fluorescing detritus, which were subsequently sized, counted and identified with the software EcoTaxa (https://ecotaxa.obs-vlfr.fr/) (Grondin, 2019). Eukaryotic picophytoplankton were enumerated in live samples by flow cytometry (Accuri C6, Becton Dickinson) (Marie et al., 1999).

The abundances of phytoplankton cells were converted to carbon biomass using allometric relationships (Menden-Deuer and Lessard, 2000) and subsequently used to estimate their contribution to the $DMSP_p$ stock using literature values for the DMSP-carbon proportion of each taxonomic group (Stefels et al., 2007). For this calculation we assumed, based on measurements performed at stations 713 and 719, that $DMSP_p$ represented 90% of the total DMSP at all stations. This result is consistent with literature values (Kiene and Slezak, 2006; Kinsey et al., 2016). We also made order-of-magnitude estimates for the $DMSP_p$ bound to detrital particles, *Phaeocystis* colonies and DMSP-producing bacteria. Further details are given in Text S3 and Table S2.

2.7. Bacterial abundance, production, and DMSP catabolism genes

Samples (1.5 mL) withdrawn from Niskin bottles were preserved with glutaraldehyde (1% final concentration) and stored at –80°C. Bacterial abundances were determined on a flow cytometer (FACSCanto, BD Biosciences) after SYBR® Green I (ThermoFisher Scientific) staining as described by Gasol and del Giorgio (2000). Bacterial production rates were measured by [H^3]-leucine incorporation (Smith and Azam, 1992). Triplicate 1.7-mL aliquots were incubated in the dark with a mixture of 50/50 (v/v) [H^3]-leucine (Perkin Elmer) and nonradioactive leucine for 4 h at in situ temperature (1.5°C). Samples with 5% trichloroacetic acid added prior to isotope addition served as a control. Saturation and time-course experiments were performed beforehand to determine the concentration of leucine and minimum incubation time. Leucine incorporation was converted to carbon production using a conservative conversion factor of 1.5 kg C (mol leucine)$^{-1}$ (Simon and Azam, 1989).

The functional genes *dddP* and *dmdA*, associated with different DMSP catabolism pathways in bacteria, were quantified by q-PCR following previously described protocols (Levine et al., 2012; Zeng et al., 2016). Briefly, universal primers dddP_874F/971R and dmdA_282F/591R were used to quantify *dddP* and *dmdA*, respectively. Quantification was performed on an AriaMx (Agilent) using SsoAdvanced Sybr Green universal supermix (BioRad). Triplicate seven-fold serially diluted standard curves, using genomic DNA from a *Phaeobacter* sp. strain presenting both genes (Genbank accession number MW504624; details will be provided elsewhere) was run on each plate. Controls with no DNA template were also run in triplicate on each plate. Single amplifications were confirmed by a melt curve for each analysis.

2.8. Data analysis and statistics

Metrics of ice cover and water mass origin were used to depict variations along the horizontal sea-surface axis. We calculated the number of open water days (OWD) at each station using the time series of remotely sensed SIC. Positive OWD indicated the days elapsed since the station became permanently ice-free (SIC < 15%), whereas negative OWD indicated the days remaining before permanent ice opening (Randelhoff et al., 2019). Stations were classified into three categories according to SIC and OWD metrics (**Tables 1** and S1). Ice-covered (ICE) stations were defined by OWD < –3d, which generally corresponded to SIC persistently higher than 85% during the 3 days ending on the day of sampling. MIZ stations were defined by $-3d \leq OWD \leq 3d$. Open water (OW) stations were defined by OWD > 3, which corresponded to SIC persistently below 15% during the 3 days ending on the day of sampling.

Water masses were depicted using the "Arctic N-P relationship" (ANP), a tracer that distinguishes the nutrient signature of Atlantic Water from that of the Pacific-derived Arctic Water. Essentially, an ANP of zero means that the NO_3^-–PO_4^{3-} pairs fall on the regression line for Atlantic Water, whereas for an ANP value of one they fall on the regression line for Pacific-derived Water (Randelhoff et al., 2019, and references therein). Stations were further classified into contiguous Arctic and Atlantic domains using a fuzzy c-means clustering algorithm based on three variables: ANP at 20 m, maximum temperature in the Atlantic Water layer, and salinity at the estimated winter convection depth (Randelhoff et al., 2019). Clustering coefficients smaller (greater) than 0.4 were indicative of the Arctic (Atlantic) domain.

Along the vertical water-depth axis, the biogeochemical setting was characterized using descriptors of vertical mixing, light penetration, biological nutrient utilization and phytoplankton biomass maxima. The mixed layer depth was calculated as the shallowest depth where sigma-t exceeded by 0.03 kg m^{-3} the value at 1 m (MLD0.03). Vertical mixing was also characterized using the "equivalent mixed layer depth" h_{BD} (Randelhoff et al., 2017). This metric was developed for meltwater-influenced surface waters

Table 2. Spearman's rank correlations between selected phytoplankton pigments and total carbon biomass proxied by the beam attenuation coefficient (c_p), $DMSP_t$ and DMS. DOI: https://doi.org/10.1525/elementa.2020.00113.t2

Pigments[a]		Phytoplankton Class[b]	Correlation Coefficients[c]		
			c_p	$DMSP_t$	DMS
Chlorophylls	Total chlorophyll *a* (TChl *a*)	All	**0.85**	**0.87**	**0.72**
	Chlorophyll *b* (Chl *b*)	**Chlorophytes, prasinophytes**, dinoflagellates (type 5)	**0.65**	**0.75**	0.39
	Chlorophyll *c2* (Chl *c2*)	Diatoms, haptophytes (type-7), most dinoflagellates, cryptophytes, **chrysophytes, pelagophytes**	**0.79**	**0.79**	**0.68**
	Chlorophyll *c3* (Chl *c3*)	**Haptophytes**, diatoms, dinoflagellates (type 2), raphidophytes, dictyochophytes	**0.45**	**0.50**	0.32
Photosynthetic carotenoids (PSC)	Fucoxanthin (Fuco)	**Diatoms, haptophytes**, chrysophytes, dinoflagellates (types 2–3)	**0.69**	**0.68**	**0.64**
	19′-hexanoyloxyfucoxanthin (Hex-fuco)	**Haptophytes** (type-7, e.g., *Chrysochromulina* spp.), **dinoflagellates** (type 2)	**0.60**	**0.75**	0.39
	19′-butanoyloxyfucoxanthin (But-fuco)	Haptophytes, **chrysophytes, pelagophytes**, dinoflagellates (type 2)	**0.53**	**0.59**	0.36
	19′-butanoyloxyfucoxanthin-like (But-fuco-like)[d]	Haptophytes (type 8; e.g. *Phaeocystis sp.*)	0.53	0.53	0.54
	Peridinin (Peri)	**Dinoflagellates** (type 1)	0.57	**0.74**	0.46
	Alloxanthin (Allo)	**Cryptophytes**, dinoflagellates (type 4)	**0.53**	**0.69**	0.36
	Prasinoxanthin (Pras)[e]	**Prasinophytes** (type 3)	**0.60**	**0.71**	0.39
Photoprotective carotenoids (PPC)	β carotene[f]	All except cryptophytes	**0.84**	**0.90**	**0.71**
	Diadinoxanthin + Diatoxanthin (DD)	Diatoms, prymnesiophytes, dinoflagellates, chrysophytes	**0.65**	**0.77**	**0.50**
	Violaxanthin + Antheraxanthin + Zeaxanthin (VAZ)	Chlorophytes, chrysophytes, prasinophytes	**0.47**	**0.73**	0.31
Degradation products	Pheophorbide *a* (Pheo *a*)	Protozoan fecal pellets	0.43	0.40	0.40

[a] Pigments are grouped according to functional and chemotaxonomic criteria following Zapata et al. (2004), Jeffrey et al. (2012), Coupel et al. (2015) and Schanke et al. (2020), and their abbreviations follow the Scientific Council for Oceanic Research (Jeffrey et al., 2012).

[b] For chlorophylls and PSC, major pigments of each algal class are indicated by highlighting the taxa in bold.

[c] All correlations are significant with $P < 0.05$, and bold face distinguishes correlations with $P < 10^{-4}$. Sample sizes are 80–118, except for But-fuco-like ($n = 58$) and Peri ($n = 72$). Underlining denotes pigments more closely associated to either $DMSP_t$ or DMS, whereas no underlining indicates similarly strong association with both compounds, according to a redundancy analysis (**Figure 2**).

[d] A 19′-butanoyloxyfucoxanthin-like pigment was found in *Phaeocystis* by Rowan (1989), and Zapata et al. (2004) reported the occurrence of an unknown 19′-butanoyloxyfucoxanthin-like pigment in haptophytes, characterized by absorption peaks shifted +1 nm from those of 19′-butanoyloxyfucoxanthin.

[e] Extremely similar correlations were found for neoxanthin, which occurs in chlorophytes and prasinophytes.

[f] Includes α + β carotene because of challenges in quantifying them separately, but α carotene is assumed to occur at much lower concentration (e.g., Ras et al., 2008).

in the MIZ and found to constrain the extent of vertical mixing better than criteria based on density or temperature thresholds (Randelhoff et al., 2019). The lower depth limit of phytoplankton growth was estimated as the depth where daily PAR was 0.415 mol photons m^{-2} d^{-1}, here referred to as the 0.415 isolume (Letelier et al., 2004). The nitracline depth was defined as the shallowest depth where nitrate concentration exceeded 1 μM, based on a linear interpolation of discrete nutrient measurements to a vertical spacing of 1 m. The depth of the subsurface

Table 3. Compilation of means (and ranges) of sea–air DMS flux (F_{DMS}) estimates[a] (μmol m^{-2} d^{-1}) in the Arctic sorted by ice-cover categories. DOI: https://doi.org/10.1525/elementa.2020.00113.t3

	Ice-Cover Category		
Reference (Region)	**ICE**	**MIZ**	**OW**
Matrai and Vernet (1997; Barents Sea)	n.a.[b]	17 (6–33), $n = 3$	33, $n = 1$
Galí and Simó (2010; Greenland Sea, Fram Strait)	n.a.	6.5 (0.5–22.5), $n = 10$	n.a.
Jarníková et al. (2018; Baffin Bay, Canadian Arctic Archipelago)[c]	n.a.	(<1–20)	(<1–80)
This study (Baffin Bay)	2.3 (0.2–6.0), $n = 10$	7.3 (1.1–17.1), $n = 13$	10.0 (1.7–25.7), $n = 12$

[a] F_{DMS} reported here were not corrected by the fraction of ice-free water surface (1 – SIC). The effect of sea ice is factored in afterward, using satellite-observed SIC (Section 2.9).

[b] Not available.

[c] Continuous underway measurements; sample size cannot be compared to other studies.

biomass maximum (SBM) was estimated from c_p profiles smoothed with a 5-point running mean to remove spikes.

To describe biogeochemical patterns along the horizontal and vertical dimensions, we calculated median profiles of selected variables for the three OWD categories (ICE, MIZ, and OW) after additional binning of the measurements into four depth (z) layers: $z \leq 9$, $9 < z \leq 21$, $21 < z \leq 41$ and $41 < z \leq 81$ m. Vertically integrated stocks were also calculated for variables measured from CTD casts (c_p) and discrete Niskin bottle profiles (DMS, $DMSP_t$, pigments). To this end, profiles were first binned (c_p) or interpolated (Niskin bottle variables) to 1-m resolution between the surface and 100 m. Discrete Niskin bottle profiles were closed by imposing a concentration of 0 at 100 m. Profiles were integrated by summation between 0 and 60 m, a range that comprised most of the phytoplankton and dimethylated sulfur stocks and sufficient discrete measurements (profiles with $n < 4$ between 0–60 m depth were not considered).

Data analyses were performed with Matlab (R2013b), python (≥3.6) and R (3.3.3; R Core Team, 2017) software. Prior to computing statistics and multivariate analyses, we tested variables for normality with the Shapiro–Wilk test. Given that none of the biogeochemical variables were normally distributed, here we generally report nonparametric statistics: median, interquartile range (IQR) and Spearman's rank correlation coefficient (r_S). However, in some instances we also report parametric statistics because they convey complementary information. In particular, means rather than medians are used to estimate fluxes at large scales because they include the effect of extreme values (see next section), and Pearson correlations (r_P) are used to evaluate linearity. We performed a redundancy analysis (RDA) with variance partitioning (Borcard et al., 2011; Oksanen et al., 2019; R package vegan) to depict the correlation structure between sulfur compounds and two sets of predictors simultaneously: physical variables and phytoplankton pigments. Finally, we used multiple linear regression with stepwise variable selection to develop empirical equations linking $DMSP_t$, DMS and F_{DMS} to their main environmental drivers. Further details on multivariate analysis are provided in Text S4.

2.9. Satellite-based estimates of DMS emission from the MIZ ($E_{DMS,\ MIZ}$)

We computed pan-Arctic $E_{DMS,\ MIZ}$ as the product of MIZ ice-free area, estimated from satellite images, and mean F_{DMS} per unit of ice-free ocean area in the MIZ, $\langle F_{DMS} \rangle$, based on a compilation of in situ studies (**Table 3**). First, pixels were flagged as MIZ or non-MIZ using the SIC time series for each pixel (see below). Second, $\langle F_{DMS} \rangle$ was multiplied by (1 – SIC) in flagged pixels to obtain maps of $F_{DMS,\ MIZ}$ (8-day and 28-km resolution). Third, the resulting flagged pixels were summed over 5° latitude bands between 65°N and 85°N and over time to obtain annual $E_{DMS,\ MIZ}$ estimates (Gg S y^{-1}).

To obtain a plausible range for $E_{DMS,\ MIZ}$, we used two different criteria ("A" and "B") for flagging pixels as MIZ. Both criteria rely on the date of permanent ice opening calculated from daily SIC time series (Renaut et al., 2018), but they differ in the duration of the MIZ period. In case A, the MIZ period was defined as the 8 days that comprised the ice opening date in a given pixel, and the corresponding mean (median) SIC was 22% (21%) at pan-Arctic scale. These two metrics (MIZ duration and corresponding ice cover) compare well with those observed during our study (**Table 1**). However, we observed that in certain areas SIC had decreased below 85% several days before permanent ice breakup. To account for the corresponding DMS emissions, in case B the duration of the MIZ period was defined by a backward search starting with the ice opening 8-day period and ending when SIC exceeded 85%, but never exceeding 32 days (to ensure that only the melt period was included). The mean (median) duration in case B was 16 (12) days, and the corresponding mean (median) SIC during the MIZ period was 36% (42%) at the pan-Arctic scale. Thus, case B allowed for geographic and interannual variations in MIZ duration, reflecting different ice-edge dynamics.

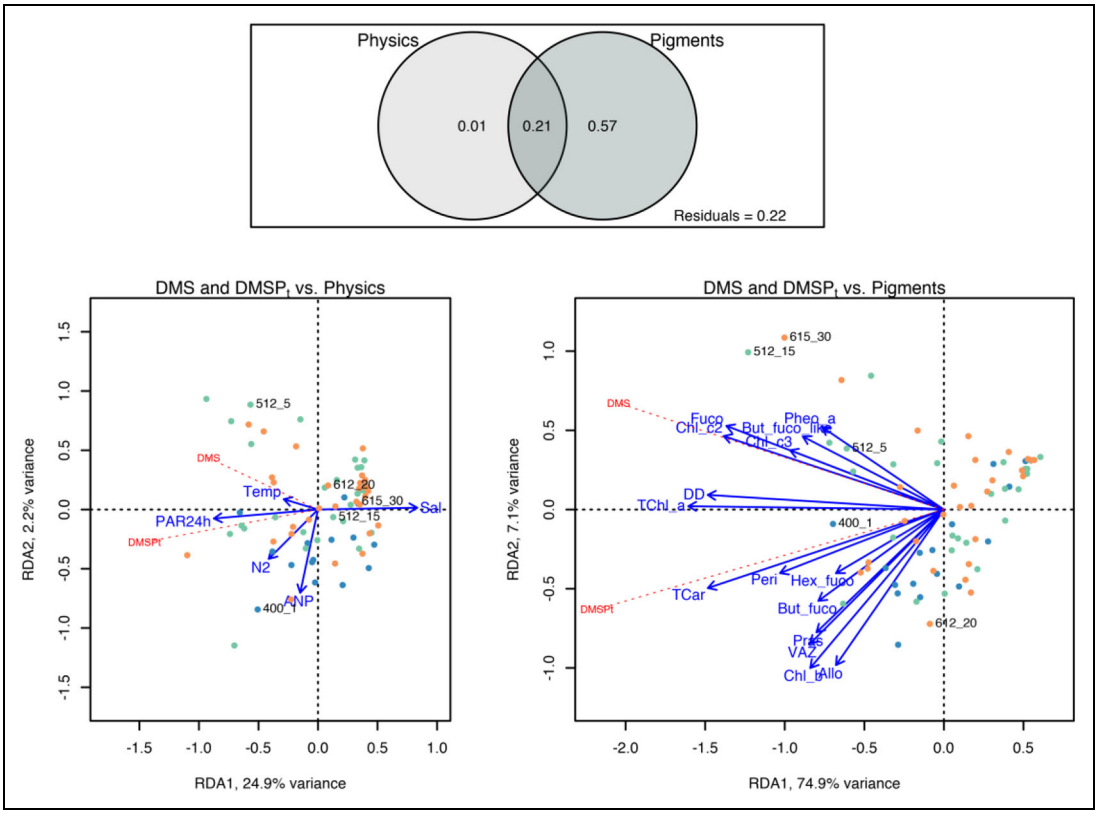

Figure 2. Redundancy analysis (RDA) between dimethylated sulfur compounds and two different sets of predictor variables. Variance partitioning plot (top), RDA triplot with physical variables only (bottom left), and RDA triplot with phytoplankton pigments only (bottom right). In the bottom plots, dots correspond to individual samples colored according to the OWD classification as in previous figures (blue for ICE, green for MIZ, orange for OW); samples with either DMS > 20 nM or DMSP$_t$ > 200 nM are identified (station_depth). DOI: https://doi.org/10.1525/elementa.2020.00113.f2

3. Results

3.1. Oceanographic and biogeochemical setting

Transect hydrography was characterized by east–west gradients in water masses and gradual ice retreat (**Figure 1**; **Table 1**). At the eastern end of the station grid, close to the West Greenland shelf, the clear signature of warm Atlantic-derived water flowing in through the Davis Strait was observed. The western end was influenced by less dense and colder waters of Pacific origin coming from the Canadian Archipelago (Tang et al., 2004). Consequently, ice retreat started in the east, with the ice edge steadily moving west at around 4 km d^{-1}. This retreat led to a parallel gradient in surface layer properties: eastern stations had sea-ice concentrations at or close to 0%, and near-surface layer (<50 m) hydrography showed substantial surface warming, whereas western stations were mostly ice-covered and showed no surface warming (Randelhoff et al., 2019). The Atlantic- and Pacific-derived water masses also had distinct nutrient signatures. In the west, the pre-bloom nutrient supply was restricted by the lower nutrient concentrations characteristic of the Arctic outflow and the strong stratification in the upper 200 m of the water column.

The development of the phytoplankton bloom tracked the east–west gradient in ice retreat and water mass distribution. Overall, phytoplankton growth was in the early stages of development in ice-covered western stations, as indicated by the near-surface nitracline and shallow SBM depths (**Table 1**; **Figure 3**). At the eastern side, the phytoplankton bloom had further developed into a mature or even post-bloom stage with considerable nutrient depletion at the time of sampling, causing a deepening of the nitracline to around 20 m (T4–T6) or even 40 m (T7). The 0.415 µE m^{-2} d^{-1} isolume was deeper than the nitracline regardless of ice cover and surface plankton biomass (**Figure 3**), resulting in the formation of a prominent SBM between 10 and 40 m at some eastern-side stations.

Distinct phytoplankton communities were found across the ice-edge transects, with biomass usually dominated by diatoms (Lafond et al., 2019). Pennate diatoms (*Fragilariopsis* spp., *Pseudo-nitzschia* spp., *Ceratoneis closterium*) were numerically dominant in the western side, whereas colonial centric diatoms (*Thalassiosira* spp., *Chaetoceros* spp.) dominated in the eastern side. Due to their larger biovolume, centric diatoms generally dominated phytoplankton biomass (accompanied by the ice diatom *Melosira arctica* and its spores at some MIZ stations). The haptophyte *Phaeocystis pouchetii* was present at background levels at different bloom stages, with a median abundance of 1.7·10^5 solitary cells L^{-1}. Yet, this species formed massive proliferations below the pycnocline at some ice-free stations along the eastern side (stations

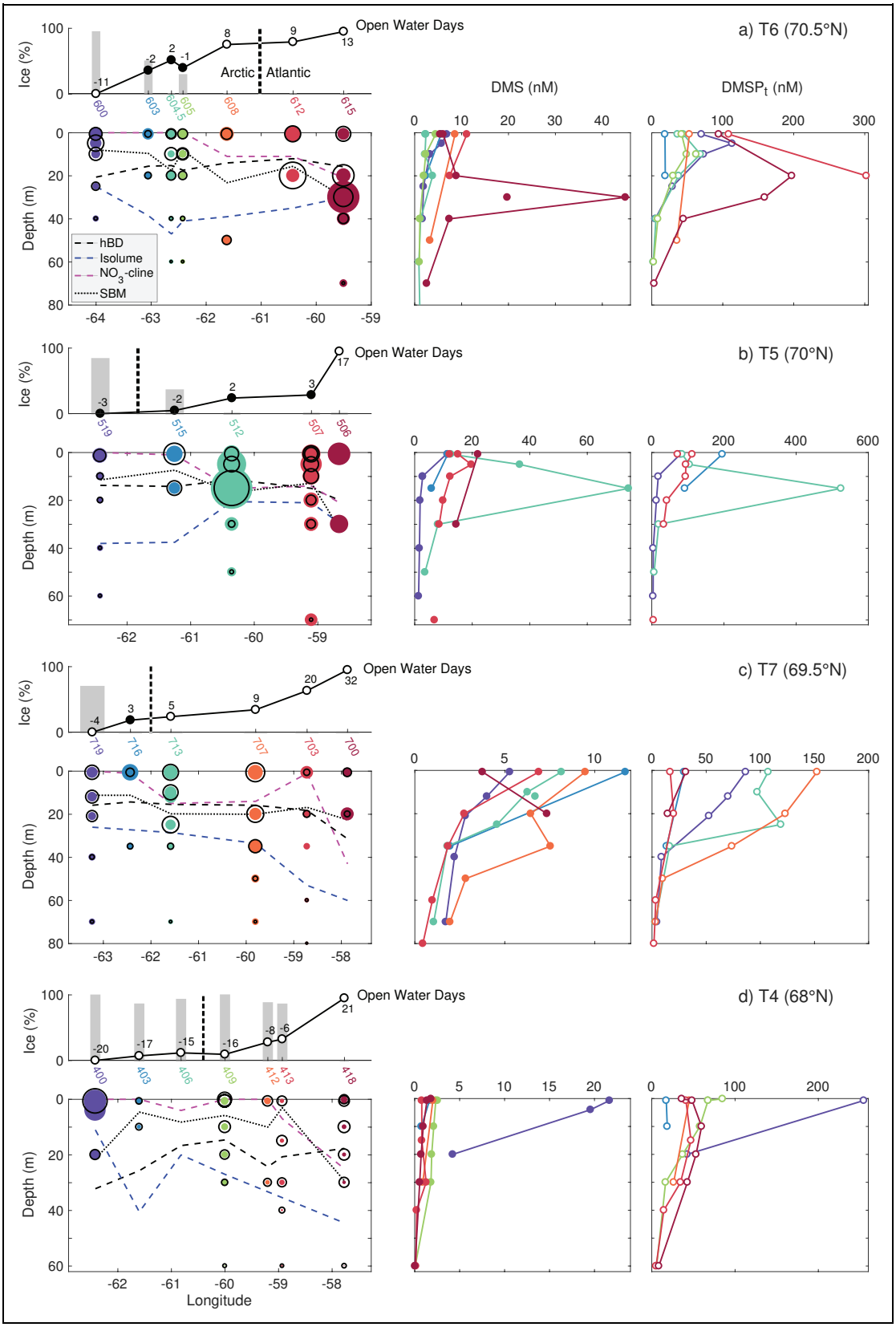

Figure 3. Vertical profiles of DMS and DMSP$_t$ and their physicochemical context. Transects are ordered by latitude. For each transect, the vertical and horizontal variability of DMS and DMSP$_t$ is illustrated with four similarly organized plots. The left bubble plots show depth-longitude transects of DMS (filled circles) and total DMSP$_t$ (empty circles with black outlines). The area of the circles is proportional to the concentration; the DMSP$_t$ circles are scaled to DMS in a 0.10 proportion (i.e., DMS and DMSP$_t$ have the same circle radius when DMS:DMSP$_t$ = 0.10 in a given sample). The superimposed lines indicate the depths of the equivalent mixed layer (h_{BD}), the PAR isolume of 0.415 mol photons m^{-2} d^{-1}, the nitracline, and the subsurface biomass maximum (see text for definitions). The plots above

512 and 615), either dominating phytoplankton biomass (station 615; $6.6{\cdot}10^6$ cells L^{-1}) or co-dominating with diatoms (station 512; $1.2{\cdot}10^7$ cells L^{-1}). Other taxa that made smaller but relevant contributions to phytoplankton biomass were haptophytes of the genus *Chrysochromulina*, athecate dinoflagellates of the genera *Gymnodinium* and *Gyrodinium* (more abundant in the eastern side), cryptophytes, chrysophytes, prasinophytes (*Pyramimonas* sp. and likely *Micromonas* sp.), dictyochophytes, and unidentified autotrophic nanoflagellates (see abundances in Figure S1).

Differences in plankton community functioning were also observed across the ice edge. Concomitant with the more advanced phytoplankton bloom stages, the ice-free, eastern-side stations with Atlantic influence were characterized by increased organic carbon recycling via the microbial loop (bacteria and microzooplankton; Saint-Béat et al., 2020). These stations generally displayed higher bacterial abundances and production (Figure S2), and hosted greater relative abundances of copiotrophic bacterial taxa (bloomers) like Rhodobacteraceae (α-proteobacteria) and *Polaribacter* (Bacteroidetes) and lower relative abundances of oligotrophic taxa like SAR11 (α-proteobacteria; J Dinasquet, unpublished data).

3.2. Spatiotemporal patterns of $DMSP_t$ and DMS

Concentrations of dimethylated sulfur compounds were usually highest in the surface layer (0–9 m), with median $DMSP_t$ and DMS concentrations of 70 and 6.3 nM, respectively. However, marked subsurface concentration maxima occurred between 10 and 30 m at some stations, and important horizontal variability and gradients were found across the four transects sampled (T4–T7), as depicted in detail in **Figure 3**. The earliest and southernmost transect, T4 (68°N), had the heaviest ice cover and the lowest DMS (<2.5 nM) and $DMSP_t$ (<90 nM) concentrations among all transects, with the stark exception of its westernmost station (400), where high $DMSP_t$ (255 nM) and DMS (22 nM) were measured just beneath the sea ice. In contrast with T4, the northernmost transects T5 (70°N) and T6 (70.5°N), which covered mostly the MIZ, showed the highest $DMSP_t$ and DMS concentrations throughout the water column. Within T5 and T6, prominent subsurface maxima were observed at 15 m at station 512 in the MIZ (524 nM $DMSP_t$; 74 nM DMS), at 30 m at station 615 in the OW (159 nM $DMSP_t$; 45 nM DMS) and at 20 m at station 612 (302 nM $DMSP_t$; no marked DMS maximum). Transect T7 (69.5°N) was sampled mostly during OW conditions except for its western end. This transect showed intermediate DMS (<12 nM) and $DMSP_t$ (<150 nM) concentrations and no prominent subsurface features.

Grouping the $DMSP_t$ and DMS profiles by ice-cover categories (**Figure 4**) revealed some general patterns. Median $DMSP_t$ profiles were remarkably similar at ICE and MIZ stations, with highest concentrations at the surface (around 70 nM) and a sharp decrease with depth that approximately followed planktonic biomass (as depicted by c_p). Median $DMSP_t$ profiles at OW stations differed slightly from this pattern, with decreased concentrations in the surface layer and increased concentrations between 10 and 41 m, indicating that subsurface $DMSP_t$ maxima became more widespread with bloom progression. Median DMS profiles showed some distinct features compared to those of $DMSP_t$: (1) a less pronounced decrease with depth at ICE stations, (2) a marked peak in median DMS concentration (12 nM) at the MIZ, and (3) a general increase throughout the water column at OW stations.

Further insights were obtained by plotting the concentrations of planktonic biomass and sulfur compounds along a continuous OWD axis (**Figure 5**). The highest near-surface DMS concentrations were generally observed between −3 and 9 OWD, and concentrations exceeding 10 nM were found in both Arctic- and Atlantic-influenced stations. Vertically integrated stocks of $DMSP_t$ and DMS peaked slightly later, between 2 and 13 OWD. At ICE stations, vertically integrated $DMSP_t$ and DMS showed little variability in both the Arctic (Pacific-influenced) or Atlantic domains. Conversely, at MIZ and OW stations the largest vertically integrated stocks of $DMSP_t$ (up to 8 mmol m^{-2}) and DMS (up to 1.4 mmol m^{-2}) were invariably found in the Atlantic-influenced stations. Large vertically integrated stocks were associated with sharp subsurface biomass maxima at stations 512 and 615, but not at stations 507, 707 and 713. Potentially different temporal evolutions of $DMSP_t$ and DMS in the Arctic versus Atlantic domains (e.g., Saint-Béat et al., 2020) could not be resolved statistically owing to limited spatiotemporal coverage.

The analyses shown in **Figures 4** and **5** offer complementary views of how physical and biological processes shaped $DMSP_t$ and DMS concentrations over the horizontal and vertical axes. To further understand how these processes differently shaped sulfur compound distributions, we performed an RDA with variance partitioning (**Figure 2**). Physical variables and phytoplankton pigments explained, jointly, 78% of the variance in DMS and $DMSP_t$ concentrations in $\log_{10}$ space, and the total variance was partitioned as follows: 57% explained only by pigments, 21% explained jointly by pigments and physical variables, and 1% explained only by physical variables. The first axis of the physics RDA explained 25% of the $\log_{10}$-variance of sulfur compounds and accounted for the vertical variation in PAR and salinity, whereas the first axis of the pigments RDA explained 75% of the $\log_{10}$-variance of sulfur compounds and accounted for phytoplankton biomass. These results indicate that bloom dynamics (i.e., phytoplankton

the bubble plots depict the percent sea-ice coverage on the day of sampling (gray bars) and corresponding open water days (black line and numbers). Filled circles distinguish stations classified as MIZ; vertical dashed lines separate Arctic and Atlantic domains (see text). The center and right plots show DMS and $DMSP_t$ vertical profiles, respectively. For all transects, each station is distinguished with a different color in the bubble and profile plots. No scale is given for DMS and $DMSP_t$ concentrations in the bubble plots, as concentrations can be seen in the profile plots. DOI: https://doi.org/10.1525/elementa.2020.00113.f3

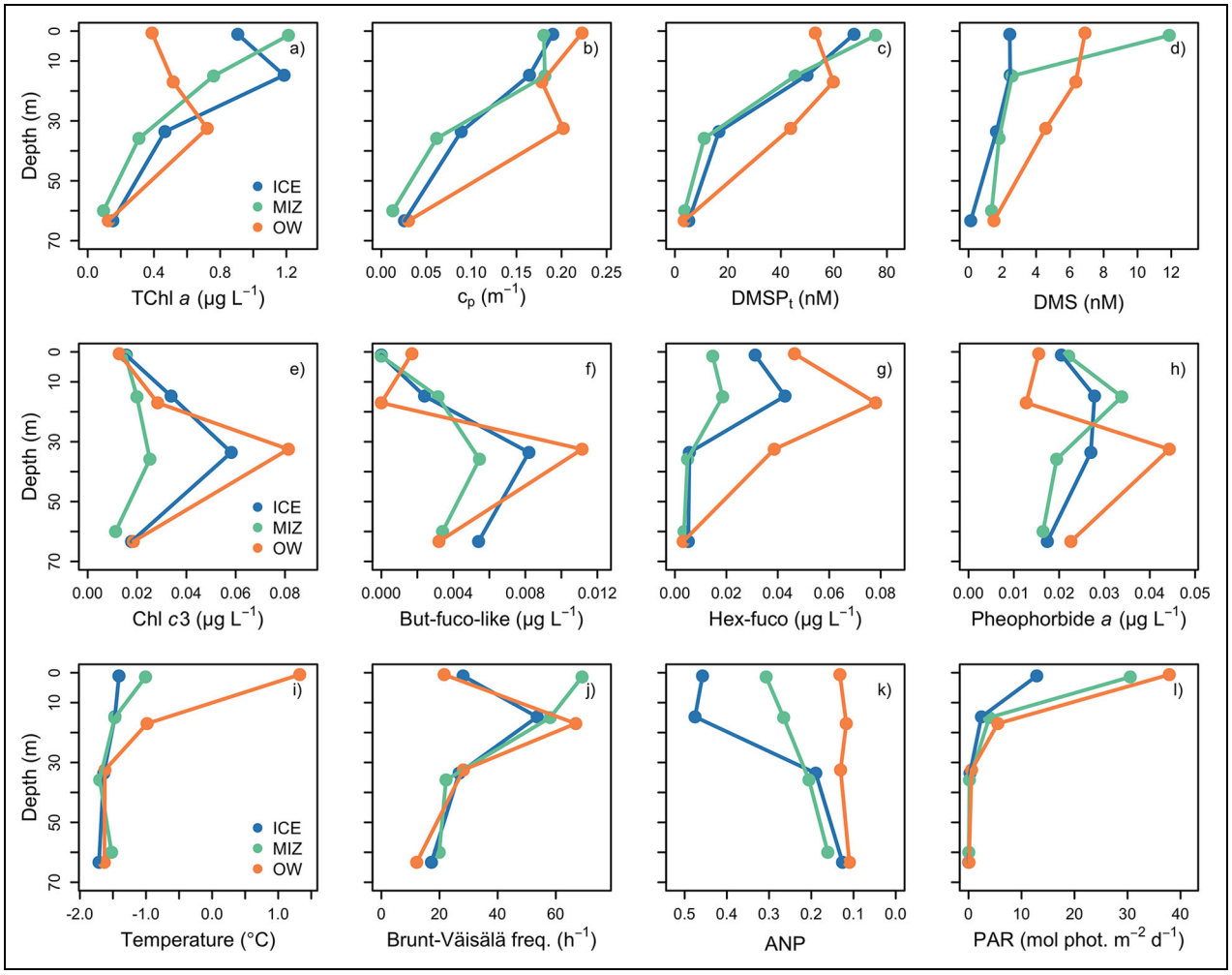

Figure 4. Median vertical profiles grouped according to ice cover and binned into 4 depth horizons. (a) Total chlorophyll *a*; (b) beam attenuation; (c) total DMSP; (d) DMS; (e) chlorophyll *c3*; (f) 19-butanoyloxyfucoxanthin-like; (g) 19-hexanoyloxyfucoxanthin; (h) pheophorbide *a*; (i) temperature; (j) Brunt-Väisälä (buoyancy) frequency; (k) Arctic N-P relationship (unitless); (l) photosynthetically active radiation. Note that the near-surface sample at station 400 was removed owing to suspected influence of ice-derived materials. DOI: https://doi.org/10.1525/elementa.2020.00113.f4

and their covariates) exerted proximate control on the sulfur compounds. The RDA also showed that phytoplankton pigments, with the exception of TChl *a* and DD, clustered with either DMS or $DMSP_t$, suggesting that different taxonomic groups (or their biogeochemical covariates) influenced DMS and $DMSP_t$ differently.

In the following two sections, we analyze in greater detail the biogeochemical factors that affect $DMSP_t$ (Section 3.3) and DMS (Section 3.4). This detailed analysis relies mostly on: (1) the correlation patterns among phytoplankton pigments, biomass, and sulfur compounds (**Table 2**; **Figures 2**, **6**, and **7**); (2) the distributions of the different variables (**Figure 4**) and their ratios (**Figure 8**) along the vertical profiles and across the ice edge; and (3) the vertical profiles of bacterial sulfur metabolism genes in the MIZ (**Figure 9**). Further analyses are presented in the supplemental materials, namely: DMSP partitioning among phytoplankton groups and other compartments (Text S3) and stepwise multiple linear regressions (Text S4.2 and Table S3).

3.3. Biogeochemical factors affecting $DMSP_t$ concentrations

$DMSP_t$ concentrations were strongly correlated to c_p, a proxy of POC and phytoplankton biomass in the euphotic layer, which explained 56% of the $DMSP_t$ variance (**Figure 6a**). A slightly lower fraction of the $DMSP_t$ variance, 52%, was explained by TChl *a* (which, indeed, was highly redundant with c_p; **Table 2**). Up to 80% of the $DMSP_t$ variance was explained by an optimal linear regression model that used as predictors five photosynthetic pigments of different taxonomic specificity plus photoprotective β carotene (Text S4.2). The $DMSP_t$:c_p ratio changed little across the ice edge or along the vertical profiles (**Figure 8a**), except for the high median ratio observed in subsurface waters at the OW stations, driven by high *Phaeocystis pouchetii* biomass. Compared to $DMSP_t$:c_p, median $DMSP_t$:TChl *a* ratios showed greater vertical variation. In the top 21 m, median $DMSP_t$:TChl *a* ratios were around 60 nmol μg^{-1} at MIZ and ICE stations and 120 nmol μg^{-1} at the OW stations (**Figure 8b**). In deeper

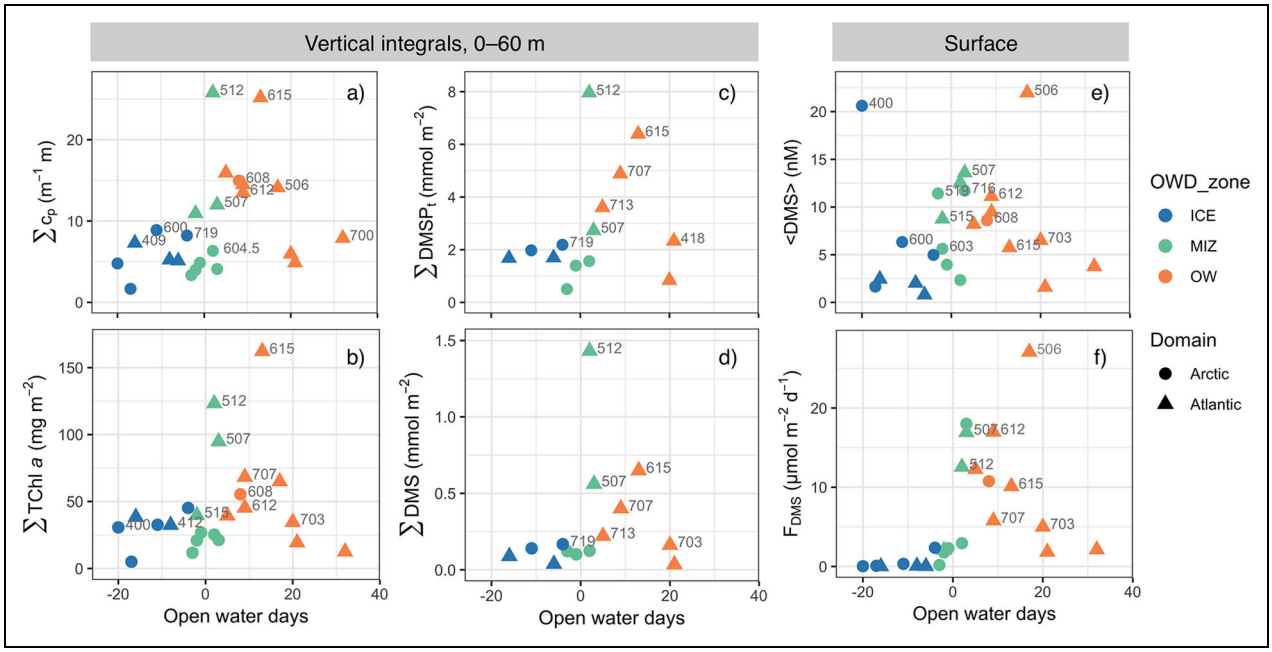

Figure 5. Evolution of biological stocks and sea–air DMS fluxes across the ice edge. Stations are classified into ice-cover categories, defined by open water days (OWD), and Arctic versus Atlantic domains. Vertical integrals correspond to (a) beam attenuation at 650 nm (c_p), a proxy of particulate organic carbon; (b) total chlorophyll *a* (TChla *a*); (c) total DMSP ($DMSP_t$); and (d) DMS. Panel (e) shows the mean near-surface (0–5 m) DMS concentration, and panel (f) the sea–air DMS flux. Station numbers are reported to the right of each symbol for data points above the first tercile (to avoid clutter). DOI: https://doi.org/10.1525/elementa.2020.00113.f5

layers, $DMSP_t$:TChl *a* ratios decreased to around 40 nmol µg^{-1}. The higher $DMSP_t$:TChl *a* ratios found closer to the surface and especially in OW can be attributed, at least partially, to the reduction of phytoplankton TChl *a* content caused by photoacclimation to high PAR (**Figure 4l**; see also **Figure 8b**, **k**, and **l**).

Phytoplankton cell counts, available at nine stations, revealed a strong positive correlation between $DMSP_t$ and the abundance of *Phaeocystis pouchetii* solitary cells (r_S = 0.82; $P < 0.05$; $r_P = 0.94$; $P < 10^{-3}$; **Figure 7a**) at the SCM. The biomass of single-celled *Phaeocystis pouchetii* accounted for up to 46% of the $DMSP_p$ (159 nM $DMSP_t$) in the SCM at the OW station 615, and 24% (524 nM $DMSP_t$) at the MIZ station 512. For all remaining available samples, solitary *Phaeocystis* accounted for <17% and <7% of the $DMSP_p$ at the SCM and the sea surface, respectively (Figure S3; Text S3). Prominent subsurface $DMSP_t$ peaks in the MIZ and OW stations co-occurred with elevated concentrations of Chl *c3* and a But-fuco-like pigment. Chlorophyll *c3* was identified by Lafond et al. (2019) as a diagnostic compound for *Phaeocystis pouchetii* in the Green Edge cruise. The But-fuco-like pigment, which occurred at lower concentrations, was suggested as a marker for *Phaeocystis pouchetii* (Rowan, 1989) or, more broadly, type-8 haptophytes (Zapata et al., 2004). Although both pigments peaked in the 21–41 m layer, they showed different distributions (**Figure 4e** and **f**) and ratios to TChl *a* (**Figure 8e** and **f**) across the ice edge (see next section). Concentrations of $DMSP_t$ were also significantly correlated to the abundance of pennate diatoms at the SCM ($r_P = 0.85$; $P < 0.01$; $r_S = 0.62$; $P < 0.10$). Weaker correlations were found for pennate diatoms at the near-surface and for centric diatoms in both the SCM and surface layers. Diatoms (pennate + centric) were likely the main DMSP producers in some samples with moderately high $DMSP_t$ (72–94 nM) in the MIZ, such as in the surface and SCM at station 507 (up to 80% of $DMSP_p$) and the surface at station 512 (up to 30% of $DMSP_p$). In the remaining samples, diatoms accounted for around 3% of the $DMSP_p$ (Figure S3; Text S3). Median Fuco:TChl *a* ratios in the top 21 m were highest in the MIZ, probably indicative of enhanced diatom biomass (Coupel et al., 2015), supporting the important role of diatoms as DMSP producers in shallow MIZ waters.

Whereas evidence suggests that *Phaeocystis* and diatoms dominated the $DMSP_p$ stock in high-biomass samples, other taxa were dominant $DMSP_p$ producers in samples with moderate-to-low biomass (Figure S3), which was especially true of dinoflagellates. Athecate dinoflagellates of the *Gyrodinium/Gymnodinium* complex contributed 30%–50% of the $DMSP_p$ at the SCM at stations 605, 707, 713, and 719. In addition, a moderate correlation was also found between $DMSP_t$ and peridinin (**Table 2**; **Figure 2**), a marker for some DMSP-rich dinoflagellates (Caruana and Malin, 2014) that reached its highest concentrations in subsurface waters at the ICE and OW stations (**Figure 4g**). However, the athecate dinoflagellates that dominated microscopic counts lacked peridinin, pointing to the role of other, unidentified dinoflagellates. Photosynthetic pico- and nanoeukaryotes contributed around 10–20% of the $DMSP_p$ in some low-biomass samples. Some of them could be identified as chrysophytes

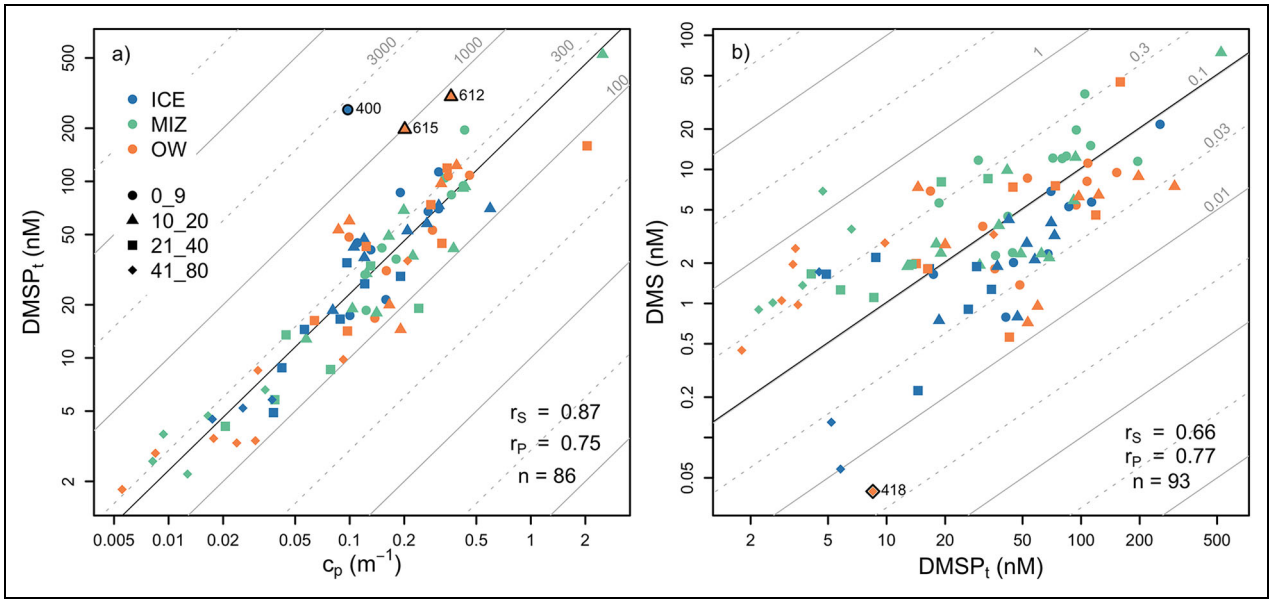

Figure 6. Scatterplots of (a) DMSP$_t$ versus c_p and (b) DMS versus DMSP$_t$. Points are colored by ice-cover categories, and symbols represent depth intervals (in meters). Outliers, defined as points beyond the first or third quartile ± 1.5 times the interquartile range, are highlighted with outer black lines and annotated with station numbers. Reference straight lines on the background mark different values of the y/x ratio (gray) and the median y/x ratio (black). Pearson and Spearman correlations (r_p and r_s; untransformed data) and sample sizes (n) are also shown. DOI: https://doi.org/10.1525/elementa.2020.00113.f6

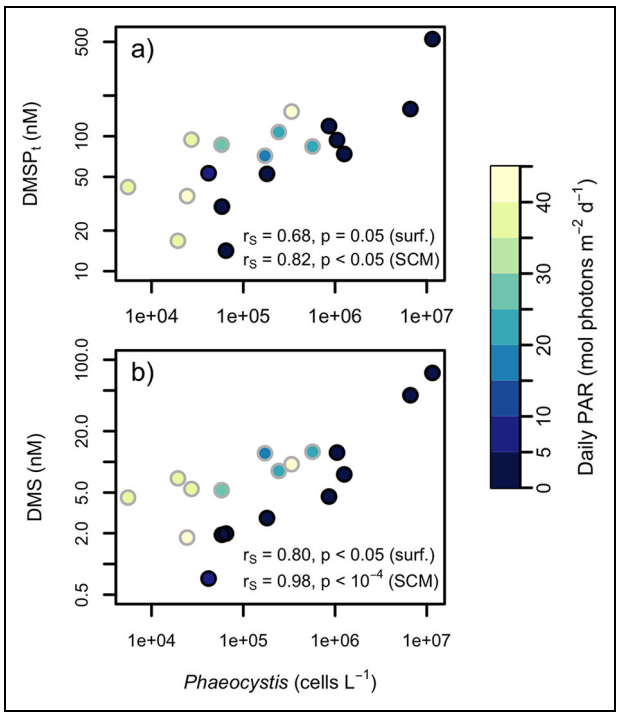

Figure 7. Relationships between *Phaeocystis* abundance and sulfur compounds in the near-surface and SCM layers. *Phaeocystis pouchetii* solitary cell abundance plotted against the concentration of (a) DMSP$_t$ and (b) DMS; the color scale depicts the mean daily irradiance, distinguishing near-surface and SCM samples. Spearman rank correlations for each sample subset are also shown. DOI: https://doi.org/10.1525/elementa.2020.00113.f7

and prasinophytes (*Pyramimonas sp.* and likely *Micromonas sp.*), and pigments characteristic of these groups (Chl *b*, But-fuco, Pras, and photoprotective VAZ pigments) clustered together in the RDA along with the cryptophyte-specific alloxanthin (**Figure 2**). Pico- and nano-sized haptophytes other than *Phaeocystis* likely contributed significantly to the DMSP pool in low-biomass conditions, as supported by the close association between Hex-fuco and DMSP$_t$ (**Table 2**; **Figure 2**) and the high median Hex-fuco:TChl *a* and DMSP$_t$:TChl *a* ratios in the top 21 m in the OW (**Figure 8b** and **g**).

The mosaic of different phytoplankton classes with contrasting intracellular DMSP concentrations resulted in limited spatiotemporal variability of the median DMSP$_t$:c_p ratio (**Figures 6a** and **8a**). Positive outliers in the DMSP$_t$ versus c_p scatterplot were found at the subsurface of the OW stations 612 and 615, concurrent with very high *Phaeocystis pouchetii* biomass, and just beneath the ice at station 400, probably indicating the release of bottom-ice biomass. Taking advantage of the linear relationship between c_p and POC, we estimated that DMSP$_p$-carbon (C_{DMSPp}) accounted for a median of 2.5% of the POC (IQR of 1.8–3.4%). Excluding an outlier (station 400 near-surface), the C_{DMSPp}:POC fraction ranged approximately between 1 and 10%, which is entirely compatible with mixed phytoplankton populations of high and low DMSP producers (Stefels et al., 2007). Indeed, this range must also encompass the DMSP bound to bacteria, detritus and zooplankton.

Our DMSP partitioning model was only partly successful at accounting for the totality of DMSP$_p$. Whereas, on average, we could account for 77%–99% of the DMSP$_p$ at

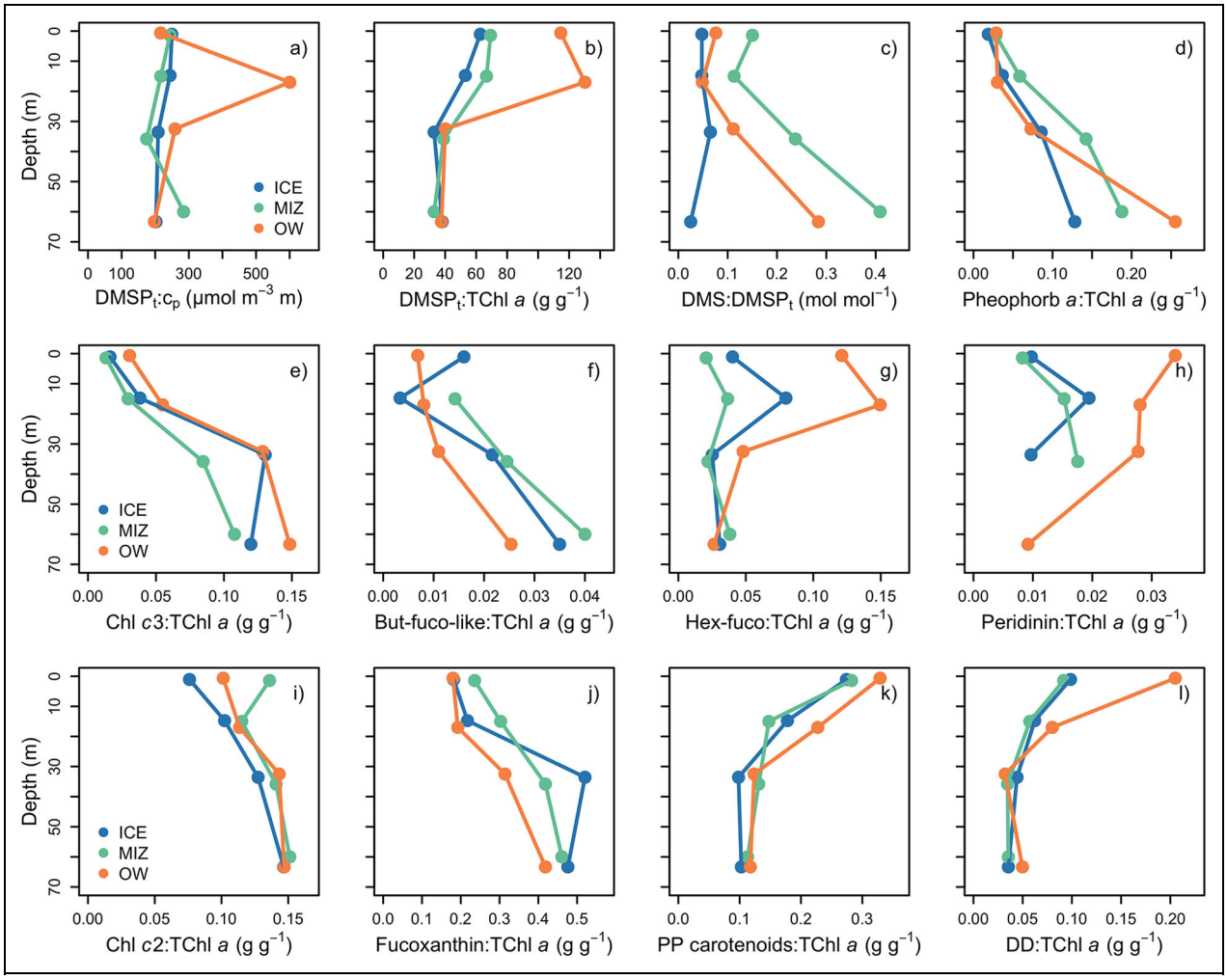

Figure 8. Vertical profiles of various median concentration ratios by ice cover and depth horizon. (a) DMSP$_t$:c_p, a proxy for DMSP$_t$:POC; (b) DMSP$_t$:TChl *a*; (c) DMS:DMSP$_t$; (d) pheophorbide *a* to TChl *a* ratio, a proxy for phytodetritus degradation linked to grazing activity; (e) Chl *c3*:TChl *a*, a proxy for *Phaeocystis pouchetii* relative abundance; (f) 19′-butanoyloxyfucoxanthin-like to TChl *a* ratio, a putative proxy for *Phaeocystis pouchetii*; (g) 19′-hexanoyloxyfucoxanthin to TChl *a* ratio (haptophytes and dinoflagellates); (h) peridinin:TChl *a* (type-1 dinoflagellates); (i) Chl *c2*:TChl *a* (chryso- and pelagophytes and other groups); fucoxanthin to TChl *a* (mostly diatoms); (k) photoprotective carotenoids:TChl *a*, a generic indicator of photoprotection; and (l) (diadinoxanthin + diatoxanthin):TChl *a* (photoprotection through the xanthophyll cycle; see **Table 2**). DOI: https://doi.org/10.1525/elementa.2020.00113.f8

the SCM (depending on the assumptions), we were able to explain only 37%–52% of the DMSP$_p$ at the near-surface (Figure S3). Although these estimates are obviously sensitive to the choice of intracellular DMSP content of each phytoplankton group, the large disagreement at the surface indicates that our reconstruction missed relevant DMSP$_p$ pools. IFCB measurements suggest that the unaccounted fraction might correspond to *Phaeocystis* colonies, fluorescing detrital particles and spores of the ice diatom *Melosira arctica*. In addition, order-of-magnitude estimates suggest a negligible contribution by DMSP-producing bacteria (likely <0.1%). Comparison between microscopic counts of single-celled *Phaeocystis* and the diagnostic pigment ratios (which should account for both colonial and single-celled *Phaeocystis*) can also shed light on this issue. According to microscopic data, the abundance of solitary *Phaeocystis* increased by 20-fold from the near-surface (median $4.3{\cdot}10^4$ cells L^{-1}) to the SCM (median $8.6{\cdot}10^5$ cells L^{-1}). In contrast, the Chl *c3*:TChl *a* and But-fuco-like:TChl *a* ratios increased approximately threefold from the surface to the SCM in the same sample subset, supporting the notion that our DMSP estimates based on single-cell counts underestimated *Phaeocystis*-bound DMSP at the surface. Unfortunately, IFCB data were not available at most stations concurrently with traditional microscopy, and their conversion into DMSP$_p$ is uncertain. Further details on DMSP$_p$ partitioning estimates are provided in Text S3.

3.4. Biogeochemical factors affecting DMS concentrations

The concentration of DMS was strongly correlated to its precursor DMSP$_t$, explaining 59% of its variance (**Figure 6b**).

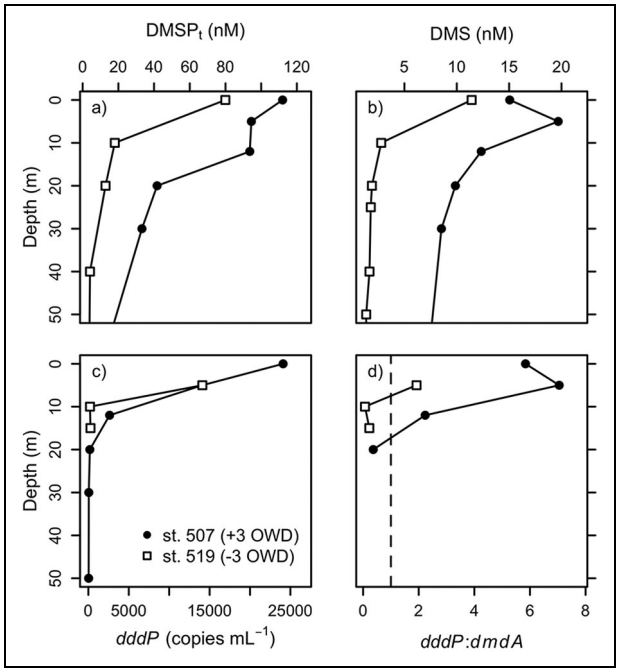

Figure 9. Inferred bacterial DMSP metabolism in the MIZ. Vertical profiles at stations 507 and 519 in the MIZ are shown for (a) DMSP$_t$ and (b) DMS concentrations, (c) abundance of the bacterial DMSP cleavage gene *dddP*, and (d) the ratio between *dddP* and the DMSP demethylation gene *dmdA*. DOI: https://doi.org/10.1525/elementa.2020.00113.f9

Strong relationships were also found between DMS and c_p ($R^2 = 0.60$) or TChl *a* ($R^2 = 0.53$; Figure S4). The highest DMS concentrations were clearly associated with a high *Phaeocystis pouchetii* abundance at the SCM, as found for DMSPt. In the subset of nine stations where microscopy counts were available, the abundance of this species was highly correlated to DMS ($r_S = 0.98$, $P < 10^{-4}$; **Figure 7b**) and explained virtually all of the DMS variance (99%) at the SCM. The relationship between *Phaeocystis* and DMS was relatively weaker in the surface layer ($r_S = 0.80$, $P < 0.05$; **Figure 7b**), pointing to a more complex interaction between various DMS production and removal pathways.

Pigment data confirmed the results based on phytoplankton counts, with the highest DMS concentrations (>20 nM; **Figure 3**) matched by the highest concentrations of the But-fuco-like pigment (>0.03 mg m^{-3}) observed at stations 400 (surface), 512 (15 m) and 615 (30 m). Up to 81% of the DMS variance could be explained with an optimal multilinear regression model using the same subset of predictor pigments as for DMSP$_t$ (except for TChl *a*; Table S3). However, unlike DMSP$_t$, a striking 94% of DMS variance was explained by adding the But-fuco-like pigment to the regression model in the subset of samples that contained it. In the RDA (**Figure 2**), pigment markers of *Phaeocystis* and other haptophytes, diatoms and grazing clustered with DMS. Markers for potential DMS producers such as type-1 dinoflagellates (Peri) and pico- or nanohaptophytes (Hex-fuco, But-fuco) clustered with DMSP$_t$, perhaps related to their higher relative abundance in samples with lower-than-average biomass and DMS (**Figure 8g** and **h**; see also stepwise regression results in Text S4.1 and Table S3).

In the absence of DMSP and DMS cycling rate measurements, the net DMSP$_t$-to-DMS conversion efficiency can be approximated using the DMS:DMSP$_t$ ratio (Galí et al., 2018), with higher ratios implying relatively fast DMS production, relatively weak DMS removal, or both. The median DMS:DMSP$_t$ ratio was 0.10, but values were scattered across two orders of magnitude (0.01–1; **Figures 3** and **6b**). The most striking feature of the DMS:DMSP$_t$ ratio was its marked increase from 0.10 at the surface to 0.30 at 60 m at the MIZ and OW stations, but not under ice (**Figure 8c**). The increase of DMS:DMSP$_t$ with depth closely paralleled proxies of *Phaeocystis* relative abundance (**Figure 8e** and **f**) and phytoplankton biomass decay and grazing intensity (**Figure 8d**), suggesting that both factors enhanced DMS yields away from the sea surface.

Beyond their clear increase with depth, DMS:DMSP$_t$ ratios showed more subtle vertical and horizontal variations (**Figure 8c**) that were not matched by *Phaeocystis* or phytodetritus proxies. First, in the MIZ and OW, median DMS:DMSP$_t$ ratios were higher in the 0–9 m layer than in the 9–21 m layer, and the difference was significant in the MIZ ($P < 0.01$; Bonferroni-adjusted Wilcoxon test). Second, median DMS:DMSP$_t$ ratios were maximal in the MIZ at all depths, even in the top 5 m of the water column (**Figure 10g**). Third, for a given *Phaeocystis* abundance, DMS was invariably higher at the surface than at the SCM (**Figure 7b**), which was not observed in the case of DMSP$_t$. These patterns cannot be explained by abiotic DMS removal processes controlling spatial distributions, because removal rates will be maximal in the surface layer and would likely increase towards the OW stations owing to stronger gas exchange and light penetration (**Figure 4l**). Therefore, variations in the net balance between biological production and consumption likely controlled the spatial distribution of the DMS:DMSP$_t$ ratio.

To further examine the role of biological processes, we explored genes associated with bacterial DMSP metabolism at several stations. Unfortunately, quantifications were performed for the first leg of the Green Edge Expedition (transects T1–T3), where DMS and DMSP were not measured, and only for stations 507 and 519 in the MIZ during the second leg described here (T4–T7; **Figure 1**). The *dddP* gene encodes for a widespread bacterial DMSP-lyase, while *dmdA* encodes for the only known DMSP demethylation enzyme, which diverts DMSP away from DMS production. Hence, the *dddP*:*dmdA* ratio should reflect the relative importance of these competing pathways, that is, it should serve as a proxy of bacterial DMS yield from dissolved DMSP. Overall, the abundance of both *dddP* and *dmdA* increased towards the top 20 m, following the vertical trend of bacterial abundance and production (Figure S2). Yet, the *dddP*:*dmdA* ratio varied widely, from median ratios ≤ 1 under ice to ratios > 3 in the MIZ and OW, suggesting that changes in bacterial DMSP catabolism could partly explain spatial patterns of DMS and DMS:DMSP$_t$. In the MIZ, the highest *dddP*:*dmdA* ratios were found in the surface layer, with a median of 3 and a maximum of 7 at station 507, concurrent with high DMS

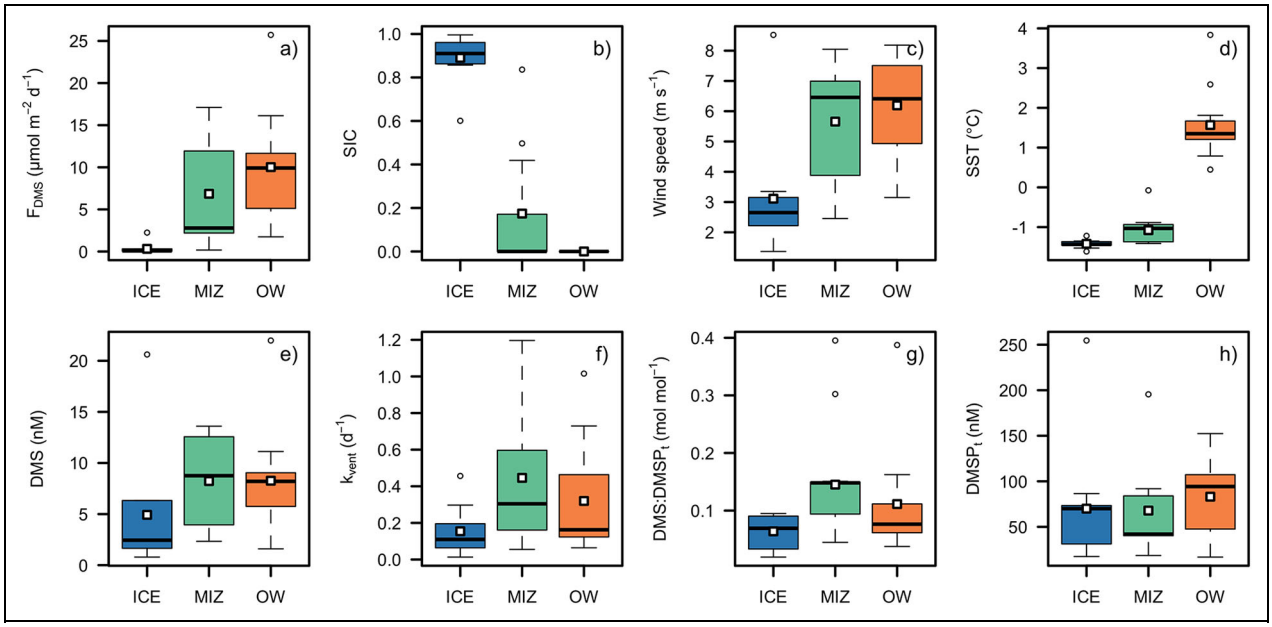

Figure 10. Sea–air DMS fluxes and corresponding controlling factors across the ice edge. (a) Sea–air DMS flux; (b) fractional sea-ice coverage (SIC); (c) wind speed; (d) sea-surface temperature; (e) near sea-surface DMS concentration (0–5 m); (f) DMS ventilation rate constants (k_{vent}) in the equivalent mixed layer (h_{BD}; see text); (g) near sea-surface DMS:DMSP$_t$ ratio (0–5 m); and (h) near sea-surface DMSP$_t$ concentration (0–5 m). Box and whisker plots distinguish between ice-covered waters (ICE), the marginal ice zone (MIZ), and open waters (OW; **Table 1**). Thick horizontal lines represent group medians and empty squares represent group means. Boxes encompass the interquartile range (IQR), and whiskers encompass measurements within $\pm$ 1.5 IQR from the median. Individual measurements outside of this range are displayed as outliers. DOI: https://doi.org/10.1525/elementa.2020.00113.f10

> 15 nM (**Figure 9**). In the OW, the highest *dddP*:*dmdA* ratios occurred in the 9–41 m layer with a median of 3–4 (data from leg 1a), in good accordance with enhanced DMS below the surface (**Figure 4d**). The *dddP*:*dmdA* ratios reported here provide a lower bound for the ratio between bacterial cleavage and demethylation genes, because as many as eight genes encoding for bacterial DMSP lyases have been described to date (Curson et al., 2011; Li et al., 2020), of which three (*dddK*, *dddP*, and *dddD*) appear to be abundant in the global surface ocean (Landa et al., 2019).

3.5. Sea–air DMS flux (F_{DMS}) and its drivers

Sea–air fluxes ranged between <0.05 and 26 µmol m^{-2} d^{-1}. When plotted on a continuous OWD axis, F_{DMS} peaked between 0 and 20 OWD, wherein it usually exceeded 10 µmol m^{-2} d^{-1}. The average F_{DMS} was highest at the OW stations, with 10.0 µmol m^{-2} d^{-1} (**Figure 10a**). Correcting for the daily fractional ice cover (i.e., multiplying the F_{DMS} from ice-free waters by 1 – SIC) decreased the mean F_{DMS} from 2.3 to 0.3 µmol m^{-2} d^{-1} in the ICE stations and from 7.3 to 6.9 µmol m^{-2} d^{-1} in the MIZ stations. However, the main driver of the increasing F_{DMS} towards OW was not the decreasing sea-ice cover, but the concomitant increase in the sea-surface DMS concentration, wind speed and SST (**Figure 10**). Among these four factors, the sea-surface DMS concentration and wind speed exerted the strongest control on F_{DMS}, together explaining 75% of the total variance in the flux data.

Assuming DMS ventilation losses affected the entire mixed layer represented by h_{BD}, DMS turnover due to sea–air exchange was typically <0.03 d^{-1} (>30 d) at the ICE stations and 0.04–0.10 d^{-1} (10–25 d) at the MIZ and OW stations. Assuming instead that ventilation affected only the shallow layer defined by MLD0.03 (**Table 1**), we obtained shorter turnover times, especially in the MIZ where the median and maximum were 0.3 d^{-1} (3 d) and 1 d^{-1}, respectively. Wind speed during the 24 h prior to sampling did not show significant correlations to the residual DMS variance, that is, the DMS variance not explained by phytoplankton biomass. Thus, ventilation did not deplete near-surface DMS appreciably.

4. Discussion

The distribution of DMSP$_t$ and DMS across the Baffin Bay receding ice edge largely followed the evolution of the phytoplankton bloom. The maximum observed DMSP$_t$ (524 nM) and DMS (74 nM) concentrations are, by far, the highest reported in the Atlantic and Canadian sectors of the Arctic to our knowledge (see compilations by Jarníková et al., 2018, and Matrai et al., 2007; Lizotte et al., 2020). Observed near-surface DMS concentrations and sea–air F_{DMS} were within the range of previous studies (**Table 3**).

In the first part of this section we analyze the relationship between the physicochemical environment and the spatiotemporal patterns of DMSP$_t$ and DMS concentrations, with the goal of inferring the main processes controlling DMS cycling and emissions across the ice edge. This analysis draws on the comprehensive description of the ecosystem (and, foremost, phytoplankton dynamics) provided by the Green Edge datasets (Lafond et al.,

2019; Randelhoff et al., 2019; Saint-Béat et al., 2020). In the second part, we present pan-Arctic estimates of present-day $E_{DMS,\ MIZ}$, and discuss the implications of changing ice cover for future DMS emissions.

4.1. DMS cycling regimes and pathways

4.1.1. *Phaeocystis pouchetii* subsurface maxima

Phaeocystis was present at fairly high background levels at most stations according to cell counts (**Figures 7** and S1) and marker pigments (**Figure 8e** and **f**), and its abundance typically increased towards the SCM. Massive *Phaeocystis* growth, however, was confined to Atlantic-influenced waters below the fresh surface layer, where the highest $DMSP_t$ and DMS concentrations were recorded (**Figures 3** and **5**). The highest *Phaeocystis* abundance found in our dataset ($1.2{\cdot}10^7$ cells L^{-1}; station 512) is, to our knowledge, a record high for Baffin Bay, and similar to the highest abundances reported so far in the Arctic ($1.2{\cdot}10^7$ cells L^{-1} in Kongsfjorden, Eilertsen et al., 1989; $1.8{\cdot}10^7$ cells L^{-1} over the Chukchi Plateau, Sherr et al., 2003; $8.7{\cdot}10^7$ cells L^{-1} over the Yermak Plateau in the Fram Strait, Assmy et al., 2017). Our estimates of *Phaeocystis* biomass are conservative because they do not include colonies (see Section 3.4 and Text S3). Wassmann et al. (2005) found that colonies made up, on average, 16% of the total *Phaeocystis* biomass in the euphotic layer in the Barents Sea and adjacent areas. In our dataset, colonial *Phaeocystis* may have represented a larger fraction of the total *Phaeocystis* biomass in the surface layer, given the large fraction of $DMSP_p$ that could not be reconstructed from available phytoplankton cell counts (Section 3.3).

Phaeocystis single-cell abundance explained an overwhelming fraction of the DMS variance in the SCM layer ($R^2 = 0.99$, $n = 9$; **Figure 7b**). Such a strong relationship is unprecedented in the literature, to our knowledge, and suggests that *Phaeocystis* DMSP-lyase activity controlled DMS production in the SCM layer, even at stations where this species did not dominate the $DMSP_p$ pool (Figure S3). Our finding is akin to the very strong association between *Phaeocystis globosa* biomass and potential DMSP-lyase activity ($R^2 = 0.97$) found by Stefels et al. (2007) during a coastal phytoplankton bloom. Still, the observed correlation does not exclude the contribution of bacterial DMSP cleavage (Figure S2). Although the positive correlation between *Phaeocystis* abundance and DMS was not as strong in the near-surface, it was significant and suggests that this species made a substantial contribution to DMS production in the surface layer.

Despite the sharp vertical DMS gradients encountered, upward diffusion of DMS from the subsurface maxima likely made a minor contribution to sea–air DMS fluxes, compared to DMS cycling in the upper mixed layer. Our order-of-magnitude calculations (Text S5) indicate that diapycnal DMS transport was generally smaller than other DMS budget terms. An exception was found at station 512, where the diapycnal DMS flux may have been comparable in magnitude to the sea–air flux, though smaller than biological and photochemical DMS turnover rates. According to current knowledge, the main fate of subsurface DMS stocks was probably the consumption by specialized methylotrophic bacteria (Vila-Costa et al., 2006; del Valle et al., 2007), capable of rapid biological DMS turnover (0.5–3 d^{-1}) in subsurface Arctic waters (Galí and Simó, 2010). Events of rapid DMS outgassing from the SCM could occur if storms were powerful enough to erode the stable pycnocline (Le Clainche et al., 2006). However, such events are unlikely to happen under high ice-melt rates typically present at the ice edge in summer (Randelhoff et al., 2019).

Understanding the dispersion mechanisms underpinning Arctic *Phaeocystis* blooms is key to assessing its role in the present and future Arctic. Abundant recent literature supports the association of *Phaeocystis pouchetii* with Atlantic waters at high northern latitudes (e.g., Galí and Simó, 2010; Metfies et al., 2016; Assmy et al., 2017; Engel et al., 2017; Kubiszyn et al., 2017; Simo-Matchim et al., 2017; Krawczyk et al., 2018; Ardyna et al., 2020), and its preference for growing below the pycnocline, in more saline and less irradiated waters (Lasternas and Agustí, 2010; Simo-Matchim et al., 2017; this study). Despite its well-established Atlantic origin, however, the median relative *Phaeocystis* abundance during Green Edge was similar across east–west transects according to marker pigments (**Figure 8e** and **f**). We hypothesize that seed populations carried by the Atlantic inflow (West Greenland Current) mixed with Arctic water masses (**Figure 1**), a process likely enhanced by submesoscale motions at the ice edge (Castro et al., 2017; Manucharyan and Thompson, 2017). In this regard, marked patchiness was evident in high resolution hydrographic data recorded during Green Edge, and also in the large variation of dimethylated sulfur concentrations registered at some stations between the morning and afternoon CTD casts (e.g., station 615, 30 m sample in **Figure 3**). Thus, water-mass mixing possibly allowed for the early initiation of the bloom under ice, perhaps connected to the colonization of bottom ice by *Phaeocystis* (see Section 4.1.3), eventually leading to a massive subsurface bloom under optimal environmental conditions. Large-scale under-ice *Phaeocystis* blooms have been observed near the Fram Strait (Assmy et al., 2017). These blooms could eventually produce very high F_{DMS} if they were rapidly advected away from the ice cover and suddenly exposed to high irradiance (Galí et al., 2013; Vance et al., 2013; Galindo et al., 2016).

4.1.2. *Phytoplankton*-bacterial connections modulated by stress in MIZ surface waters

In the surface layer of the MIZ, high DMS concentrations and relatively high DMS:$DMSP_t$ ratios possibly resulted from the multiplicative effects of enhanced DMSP and DMS release by phytoplankton (Sunda et al., 2007; Galí et al., 2013) and enhanced bacterial DMS yields from the microbial consumption of DMSP (Slezak et al., 2007). Utilization of DMSP by the free-living bacterial community clearly increased towards the surface, and the highest ratios between the potential cleavage and demethylation activities (*dddP*:*dmdA*) were found in the top 10 m of the water column in several MIZ and some OW stations (**Figures 9** and S4). High bacterial DMS yields are a response

to the oversupply of reduced sulfur, allowing bacteria to retain the carbon moiety of DMSP while releasing the sulfur as DMS (Kiene et al., 2000; Varaljay et al., 2015; Galindo et al., 2015).

Phytoplanktonic DMSP has to be released to the extracellular medium to be usable by bacteria. Because zwitterions like DMSP cannot passively cross healthy cell membranes, DMSP release must result from cell breakage by grazers, cell membrane damage, or active exudation through membrane transporters or secretory vesicles (Stefels et al., 2007; Orellana et al., 2011). Release of DMSP through zooplankton grazing was likely heightened in mature bloom stages in OW (Saint-Béat et al., 2020), probably accompanied by viral lysis (Malin et al., 1998) and autolysis. In contrast, release of DMSP upon radiative damage was likely important in the MIZ surface layer, as previously observed experimentally by Galindo et al. (2016). In support of this hypothesis, Alou-Font et al. (2016) observed that around 20% of the phytoplankton cells in the Arctic surface layer had permeable (compromised) membranes for daily PAR between 20–40 mol photons m^{-2} d^{-1}, and this fraction exceeded 50% for daily PAR > 50 mol photons m^{-2} d^{-1}. Median (maximum) daily PAR levels of 31 (35) and 38 (52) mol photons m^{-2} d^{-1}, respectively, were recorded in MIZ and OW stations during our cruise (**Figure 4l**). Despite the much higher light levels in the MIZ and OW surface layers, the major photoprotective pigments were not upregulated in the MIZ compared to ICE stations (**Figure 8k** and **l**), whereas a distinct photoprotective response was found in the OW stations. Thus, insufficient photoprotection might have favored DMSP release by MIZ phytoplankton. Finally, the enhanced availability of algal substrates can also be inferred from the high bacterial abundance and production in the 0–21 m layer in the MIZ (Figure S4).

High DMSP availability in the MIZ may have also resulted from upregulated DMSP synthesis in diatoms as a consequence of nutrient and radiative (ultimately oxidative) stress (Sunda et al., 2002; McParland and Levine, 2019). Diatoms made up a substantial fraction of the phytoplankton community in the 0–21 m layer in the MIZ according to pigment ratios (**Figure 8i** and **j**). As described in Text S3, a DMSP content of 0.4% of cell carbon in diatoms (Stefels et al., 2007) was insufficient to reconstruct DMSP concentrations during Green Edge. A higher DMSP-carbon content of 2% provided a better fit, and an even higher content was compatible with observed near-surface $DMSP_t$ concentrations. On the other hand, diatoms may also obtain antioxidant DMSP through uptake (Theseira et al., 2020), a pathway that is enhanced under high irradiance (Ruiz-González et al., 2012) and that diverts DMSP from DMS production.

In addition to boosting DMS production through the coupled activities of phytoplankton and bacteria, nutrient and radiative stress in the MIZ and OW surface layer likely enhanced direct DMS release by phytoplankton (Sunda et al., 2002; Sunda et al., 2007). UVR may have partially offset the increase in bacterial DMS production via photoinhibition of DMSP uptake (Slezak et al., 2007), while simultaneously inhibiting bacterial DMS consumption (Toole et al., 2006; Galí and Simó, 2010). In any case, the net effect of interacting DMS production and consumption pathways was a peak in DMS concentrations in the stably stratified surface layer of the MIZ (**Table 1**; **Figure 4**).

4.1.3. Ice-water exchange

Very high concentrations of $DMSP_t$ (255 nM) and DMS (22 nM) were found beneath the ice at station 400, concurrently with an anomalously high $DMSP_t$:c_p ratio (**Figure 6a**) and But-fuco-like concentration. This outlier observation (see **Figure 3**) suggests that *Phaeocystis* grew in and was released from bottom sea ice, adding to scarce previous reports of *Phaeocystis* colonizing sea-ice environments (Fernández-Méndez et al., 2018; Selz et al., 2018). Spores of the ice diatom *Melosira* were also found in the water column, in particular at the SCM of stations 512 (MIZ) and 703 (OW), and potentially contributed to the DMSP pool. Galindo et al. (2014; Galindo et al., 2015) observed that, at the onset of the melt season, snow melting caused ice drainage events that flushed ice-bottom biomass and seeded the pelagic diatom bloom, boosting bacterial DMSP cycling beneath the sea ice. If *Phaeocystis* was present in the sea ice, such a process could further enhance DMS production and eventual outgassing.

To further explore the role of ice melt in supplying dimethylated sulfur compounds to the upper water column, we analyzed the correlation between several variables and salinity, repeating the analysis in progressively thicker layers from 0–5 m to 0–41 m (Figure S5). The correlation between DMS and salinity became more negative as shallower layers were considered, reaching $r_S = -0.49$ ($P < 0.05$) in the 0–5 m layer. Other variables ($DMSP_t$, TChl *a* and c_p) showed similar but nonsignificant patterns, whereas *Phaeocystis* diagnostics (Chl *c3*, But-fuco-like) were positively correlated to salinity but only if a deeper layer (0–41 m) was considered. The significantly negative correlation between salinity and near-surface DMS may be seen as supportive of the role of ice-released organic matter; however, this correlation was clearly weaker than that found between DMS and *Phaeocystis* (**Figure 7b**). Moreover, an important role of sea ice in directly supplying DMS or its precursors to near-surface waters during Green Edge is at odds with other observations. First, surveys covering a longer period of the melt season indicated that the majority of ice-bound DMSP (Galindo et al., 2014) and POC (Amiraux et al., 2019) was released to the water column well before permanent ice breakup. In the coastal Baffin Bay, the fraction of ice-derived POC was typically less than 5% in the top 10 m of the water column during the three weeks preceding ice opening (Amiraux et al., 2019). Second, model results (Hayashida et al., 2020) also indicate that ice-released DMSP is unlikely to fuel ocean-emitted DMS during the advanced melt season; yet, it could have fueled DMS emission in May, during the bottom-ice algal bloom.

4.1.4. Detrital matter

The increase in DMS:$DMSP_t$ with depth paralleled the increase in pigment markers for both *Phaeocystis* and

phytodetritus (**Figure 8d–f**). The latter is consistent with the high abundance of large marine snow aggregates in the MIZ and OW found during Green Edge by Trudnowska et al. (2021). Our observation suggests that (1) efficient DMSP-to-DMS conversion occurred in suspended and sinking particles below the euphotic layer (depth > 40 m), and (2) this DMS production was not fully balanced by increased biological DMS consumption. Increased DMSP cleavage may have resulted from both phytoplanktonic and bacterial DMSP-lyase activities, combined with particle processing by zooplankton. The few available studies indicate that large aggregates and marine snow may be a hotspot for both DMSP cleavage (Scarratt et al., 2000) and demethylation (Steiner et al., 2019) and for DMS bioconsumption (del Valle et al., 2009) in productive marine settings where particle-attached lifestyles tend to be more prevalent (Teeling et al., 2012). Moreover, bacterial groups with affinity to particles such as Bacteroidetes, gammaproteobacteria and some alphaproteobacteria (Teeling et al., 2012; Fernández-Gómez et al., 2013) can harbor several DMSP lyase genes (Curson et al., 2011; Zeng et al., 2016).

Particle sinking removes DMSP from the surface layer where it could potentially fuel DMS emissions. The importance of this process depends on the sinking-speed spectrum of DMSP-bearing particles, relative to biological DMSP turnover in the surface layer. Lizotte et al. (2008) found that less than 2% d^{-1} of $DMSP_p$ sank from the bottom of the euphotic zone during the decay of the Northwest Atlantic diatom bloom. Studies of *Phaeocystis pouchetii* blooms generally found low vertical export efficiency (Reigstad and Wassmann, 2007; Assmy et al., 2017), although export occasionally may be enhanced by processes other than gravitational sinking, e.g. water-mass subduction (Rellinger et al., 2009). During Green Edge, the vertical patterns of DMS:$DMSP_t$ and marker pigments suggest relatively slow sinking and rapid breakdown of DMSP-bearing aggregates, which altogether would attenuate the gravitational DMSP flux.

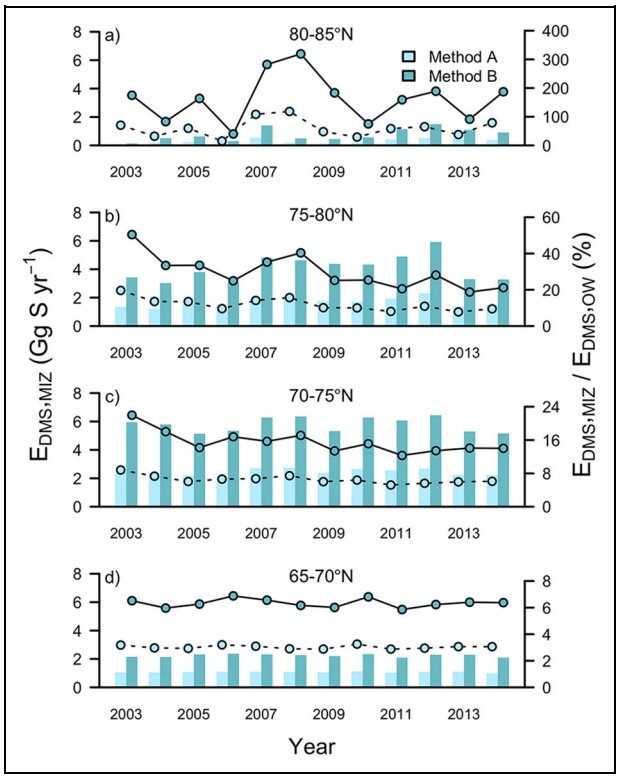

Figure 11. Evolution of Arctic MIZ DMS emission during summer (May–August) aggregated by 5° latitude bands. Bars represent DMS emission from the MIZ ($E_{DMS,\ MIZ}$; left axis); lines represent the additional percentage of E_{DMS} from the MIZ compared to OW (right axis). Colors represent methods A (light cyan) and B (dark cyan) used to compute MIZ extent (see Section 4.2). The left y-axis scale is the same in all panels to facilitate comparisons of the magnitude of $EDMS_{MIZ}$ among latitude bands, whereas right y axes scales differ because the percentages span two orders of magnitude. DOI: https://doi.org/10.1525/elementa.2020.00113.f11

4.2. Present and future E_{DMS} from the MIZ: Physical and biological constraints

The DMS fluxes measured in the MIZ during Green Edge are within the range of previous studies in the Arctic MIZ (<1–33 µmol m^{-2} d^{-1}), and the compilation in **Table 3** suggests that the mean F_{DMS} from ice-free waters in the MIZ is typically between 5 and 10 µmol m^{-2} d^{-1}. This range is consistent with the F_{DMS} diagnosed from satellite ocean color data immediately after ice opening in several Arctic subregions (Galí et al., 2019). Given that estimated mean F_{DMS} from ice-free waters between May and August at latitudes >70°N was ≤2 µmol m^{-2} d^{-1} (Galí et al., 2019), phytoplankton blooms in the Arctic MIZ can be qualified as DMS emission hotspots. In the aerosol-poor summer Arctic atmosphere, episodes of high $F_{DMS,\ MIZ}$ can easily exceed aerosol nucleation thresholds (Leaitch et al., 2013; Collins et al., 2017; Dall'Osto et al., 2017). The episodic and patchy nature of DMS flux from the MIZ is an important attribute regarding aerosol nucleation events, as recently highlighted by Webb et al. (2019) in a study of the West Antarctic Peninsula. These attributes may partly explain the episodic spikes in DMS concentrations just above the sea surface reported in Baffin Bay and the Canadian Arctic (Mungall et al. 2016; Ghahremaninezhad et al., 2019).

No published estimates of pan-Arctic $E_{DMS,\ MIZ}$ are available, to our knowledge, in spite of their importance for high Arctic aerosols. Assuming a mean F_{DMS} in ice-free MIZ waters of 5 µmol m^{-2} d^{-1}, pan-Arctic $E_{DMS,\ MIZ}$ between 2003 and 2014 would amount to a mean (±standard deviation, $n = 12$) of 5.4 (±0.6) Gg S yr^{-1} in scenario A (where the duration of the MIZ status is fixed at 8 days for any given pixel) and 12.9 (±1.6) Gg S yr^{-1} in scenario B (which allows for variable duration of the "MIZ period" for any given pixel and year; **Figure 11**). In both scenarios, the 70–80°N latitude band would account for 75% of the total $E_{DMS,\ MIZ}$ north of 65°N. We also computed the weight of $E_{DMS,\ MIZ}$ relative to open water EDMS ($E_{DMS,\ OW}$) in June and July as 100 x $E_{DMS,\ MIZ}$/$E_{DMS,\ OW}$. The additional contribution of $E_{DMS,\ MIZ}$ increases with latitude, from a modest 3%–6% (means of A–B scenarios) in the 65–70°N band to 60%–162% in the 80–

85°N band. Our estimates also suggest a temporal increase in the magnitude of $E_{DMS,\ MIZ}$ of about 10 ± 4% yr^{-1} ($P < 0.05$) between 2003 and 2014 north of 80°N, with highest $E_{DMS,\ MIZ}$ in years with record-low sea-ice extent (2007 and 2012; **Figure 11a**). This increasing trend is consistent with the progressive widening of the MIZ in summer detected until 2011 (Strong and Rigor, 2013). Our estimates are admittedly crude and should be refined as new field measurements become available. Large uncertainty arises from assigning a fixed F_{DMS} to all pixels flagged as MIZ, and future statistical upscaling exercises should take into account spatial variations in sea-surface DMS concentrations across contrasting Arctic biogeochemical regimes.

Ice melting and water-column stratification are poised to play an increasingly critical role in controlling Arctic E_{DMS}. The stability of stratification has numerous biogeochemical ramifications as it controls, at least: (1) phytoplankton productivity, through turbulent nutrient supply (Randelhoff et al., 2020), and ensuing nutrient stress that can boost DMSP production by low DMSP producers such as diatoms (McParland and Levine, 2019); (2) mean PAR and UVR exposure of the entire food web in the upper water column, and therefore radiative stress-driven DMSP and DMS cycling (Galí and Simó, 2010; Galí et al., 2013; Vance et al., 2013); and (3) CO_2 solubility and invasion of deeper waters, and thus the carbonate system parameters and pH, with potentially important effects on sulfur cycling (Hussherr et al., 2017; Hopkins et al., 2020; Bénard et al., 2021). In addition, better understanding is needed of ice-water biogeochemical fluxes and biogeochemical transformations of ice-released organic matter (Galindo et al., 2014; Hayashida et al., 2020). Physicochemical processes that alter the near-surface turbulence can further amplify the uncertainty in MIZ DMS emissions. Examples include the turbulence generated by ice drag, and the formation of freshwater lenses and sea-surface microlayers enriched in surfactants, damping near-surface turbulence (Carpenter et al., 2012).

Over large spatiotemporal scales, uncertainty in present-day and future estimates of $E_{DMS,\ MIZ}$ may also arise from changes in plankton biogeography. In this regard, knowledge of the ecological niches occupied by the main blooming groups, that is, diatoms and *Phaeocystis pouchetii*, is key. Available data tie *P. pouchetii* to the Atlantic inflow at high northern latitudes, with a growth optimum between 1°C and 5°C (Brun et al., 2015), likely warmer than that of some Arctic diatoms (Lacour et al., 2017). Others have suggested that *P. pouchetii* does not grow well in meltwater-influenced surface waters (Lasternas and Agustí, 2010) and, interestingly, decreased growth at low salinities was reported for its austral relative *P. antarctica* (Kameyama et al., 2020). Despite its apparent preference for relatively low irradiance (Simo-Matchim et al., 2017; this study), other field data suggest that this species features extremely wide photophysiological plasticity, as it can grow efficiently at both low (2 mol photons m^{-2} d^{-1}; Assmy et al., 2017) and high (40 mol photons m^{-2} d^{-1}; Cota et al., 1994) irradiance. This plasticity, the ability to use regenerated nitrogen forms (Sanderson et al., 2008), no silicate requirement (Ardyna et al., 2020), the protection from zooplankton predators provided by mucilaginous colonies (Long et al., 2007; Verity et al., 2007), and even allelopathy (Hansen and Eilertsen, 2007) may explain the ability of *Phaeocystis* to outcompete diatoms and form massive blooms under certain conditions. The northward expansion of *Phaeocystis* along with Atlantic waters in the Barents Sea detected by remote sensing (Orkney et al., 2020), analogous to that of its temperate relative *Emiliania huxleyi* in subpolar waters, indicates ongoing floristic shifts are impacting Arctic E_{DMS}. Still, what factors control *Phaeocystis* abundance and eventual dominance elsewhere in the Arctic remains unknown.

5. Conclusions and outlook

The Arctic MIZ can produce strong DMS emission pulses (**Table 3**), which can influence aerosol formation and properties in the clean Arctic summer atmosphere (Abbatt et al., 2019). Although their pan-Arctic magnitude is still uncertain (likely 5–13 Gg S yr^{-1}), these emissions cannot be overlooked and the biogeochemical factors that control them deserve further study. Productive polar ice edges like the one described here are paradigmatic of the bloom regime, whereby phytoplankton biomass is a strong predictor of dimethylated sulfur dynamics (Toole and Siegel, 2004). Here we attempted to dissect the bloom regime, which allowed us to infer a number of co-occurring DMS cycling pathways linked to different autotrophic and heterotrophic activities. Their spatiotemporal distribution was related to processes that shape the development of the late spring bloom in Baffin Bay, namely, the W–E gradient between Arctic (Pacific-derived) and Atlantic water masses, ice melting, and their combined effects on the diverging vertical gradients of light and nutrient availability (Lafond et al., 2019; Randelhoff et al., 2019; Saint-Béat et al., 2020).

Below we summarize the main findings of our study:

- **Water masses**. Extremely high biomass of *Phaeocystis pouchetii* in the subsurface biomass maximum, along with very high $DMSP_t$ and DMS, were associated unambiguously with Atlantic-influenced waters. Marked spatial patchiness in planktonic biomass and biogenic sulfur concentrations were observed in the mixing zone between the Arctic and Atlantic water masses.
- **Temporal evolution**. A single space-for-time axis, based on the open water days (OWD) metric, captured major features of the temporal evolution of the planktonic biomass and dimethylated sulfur concentrations, from bloom initiation under the ice to its peak in the MIZ and decay in open waters.
- **DMSP producers and particulate fractions**. Pigment markers for phytoplankton taxonomy and photoacclimation explained

80% of $DMSP_t$ variance. The contribution of different DMSP producers changed progressively from samples with very high $DMSP_t$ (*Phaeocystis*-dominated), moderate $DMSP_t$ (diatoms, dinoflagellates) and low $DMSP_t$ (dinoflagellates, non-*Phaeocystis* pico- and nanoeukaryotes). Particulate DMSP represented 1–10% of the POC. Detrital matter, zooplankton biomass and perhaps ice-released particles may have accounted for a substantial $DMSP_t$ fraction in some samples.

- **Microbial DMS cycling pathways**. Meltwater stratification caused the vertical segregation of sulfur cycling pathways linked to different auto- and hetetrotrophic processes. In the surface layer of the MIZ (and to some extent OW) we inferred high DMSP-to-DMS conversion via phytoplankton-bacterial interactions, likely favored by nutrient and light stress, ultimately leading to high median DMS:$DMSP_t$ ratios (0.15) and DMS concentrations (12 nM). Conversely, *Phaeocystis pouchetii* drove DMS production in subsurface biomass maxima. Efficient DMSP-to-DMS conversion was inferred in suspended or sinking aggregates below the euphotic layer, concurrent with a clear pigment signature of grazing.

Given the wide range of environmental conditions sampled during the Green Edge cruise, we argue that our findings, and the new questions they have raised, are relevant for other regions in the Arctic. Although our study is limited by the descriptive nature of the dataset, it provides a good template for upcoming process studies and modeling efforts and will be useful to refine existing conceptual models. Below we conclude by listing potential research priorities for future studies:

- **Sulfur budgets**. Comprehensive measurements of biological DMS production and consumption rates are needed to constrain DMS budgets and sea–air fluxes in relation to plankton and ice-melt dynamics. Special emphasis should be placed on (1) the microbial processes occurring in and around particles across the entire size spectrum (cells, excretion vesicles, colonies, metazoan zooplankton and large detrital aggregates), (2) ice–water mass fluxes, and (3) the modulation of sulfur budgets by interacting environmental stressors (Galí et al., 2013; Hopkins et al. 2020).
- **Phytoplankton biogeography and biogeochemical regimes**. Further field and lab work is required to understand the ecological niche occupied by *Phaeocystis pouchetii* to predict its fitness and prevalence in the future Arctic compared to diatoms. Dinoflagellates and picoeukaryotes should be included in global compilations and ecological niche studies (e.g., Brun et al., 2015). The latter groups may contribute disproportionately to the background (non-bloom) levels of $DMSP_t$ and DMS production in polar environments, and some can play a dual role acting as grazers (Stoecker et al., 2017). The response of plankton communities to decadal- or centennial-scale environmental changes (AMAP, 2017; IPCC, 2019; Inness et al., 2020) is poorly understood.
- **Repeat surveys and exploration**. Continuation of survey programs in areas with long historical records is key to detecting trends driven by climate change. Studies in undersampled regions (Central Basin and Siberian shelves, e.g., Uhlig et al., 2019; Schanke et al., 2020) are needed to upscale in situ measurements and generalize current knowledge. The transition toward a first-year Arctic ice cap may favor a high-DMS MIZ such as the one described here in contrast to the low DMS concentrations associated with multi-year ice margins (Lizotte et al., 2020).
- **Modeling**. Biogeochemical modeling studies should place emphasis on the ability to reproduce (1) the large-scale distribution patterns of key phytoplankton groups (Wang et al., 2015), (2) the vertical segregation of plankton communities and sulfur-cycling regimes, and (3) biogeochemical fluxes between sea ice and water (Hayashida et al., 2020). These modeling efforts will better constrain the $E_{DMS,\ MIZ}$ estimates presented here (**Figure 11**) and allow for future projections, regional and pan-Arctic, of DMS emissions.

Data accessibility statement

Data are deposited in the LEFE CYBER Database (http://www.obs-vlfr.fr/proof/) and can also be provided by the corresponding author M.G. on request. Scientific code for the analysis and plotting of DMS(P) data is publicly available at https://github.com/mgali/GreenEdge. Scientific code for the analysis of physical data made by Randelhoff

et al. (2019) is available at https://www.doi.org/10.5281/zenodo.2653855.

Supplemental files

The supplemental files for this article can be found as follows:

This article is accompanied by a Supplemental Material file that contains five subsections of text (S1–5), five figures (S1–S5) and three tables (S1–S3).

Acknowledgments

We are thankful to the officers and crew of the CCGS *Amundsen*, Jean-Éric Tremblay and Flavienne Bruyant for assuring the smooth development of the Green Edge expedition. We are indebted with Guillaume Massé for providing the GC-MS instrument and technical advice, and with the entire Green Edge for providing the core dataset: Joséphine Ras and Annick Bricaud (HPLC), Pierre-Luc Grondin, Philippe-Israel Morin and Joannie Ferland (IFCB), Augustin Lafond (diatom biomass), Dominique Marie and Daniel Vaulot (bacteria and picoeukaryote abundances), Fabien Joux (bacterial production), Brent Else and Tonya Burgers (meteorological data), and Philippe Massicotte (data synthesis). Thanks are extended to Guillaume Léguen for fieldwork support. We thank Alison Webb, two anonymous reviewers, and editor Jody W. Deming for constructive criticisms that improved the paper.

Funding

We acknowledge funding from AGAUR (Generalitat de Catalunya) Beatriu de Pinós postdoctoral fellowship program (MG), the Canada Excellence Research Chair in Remote Sensing of Canada's New Arctic Frontier (MB), the Canada Research Chair on Ocean Biogeochemistry and Climate and an NSERC Discovery Grant Program and Northern Research Supplement Program (MLe), NETCARE (NSERC Climate Change and Atmospheric Research program, MLe), the U.S. National Science Foundation (NSF-OCE 1756907, DJK), Marie Curie Actions-International Outgoing Fellowship (PIOF-GA-2013-629378, JD), and ArcticNet (The Network of Centres of Excellence of Canada). This is a contribution to the research program of Québec-Océan and the Takuvik Joint International Laboratory (CNRS-France & Université Laval-Canada).

Competing interests

The authors declare no conflict of interest.

Author contributions

MG collected and analyzed DMS(P) samples onboard, analyzed data, and wrote the manuscript with significant input from MLi, DJK, and AR, and contributions from all coauthors.

Designed the DMS(P) sampling strategy: MG, MLi, MLe.

Analyzed DMSP on land: LX, DJK, RH, MLi.

Provided the analysis of the physical setting: AR.

Conducted the sampling and analysis of bacterial abundance and activities: JD.

Provided satellite estimates of ice opening dates: ER.

Led the Green Edge project: MB.

References

Abbatt, JPD, Leaitch, WR, Aliabadi, AA, Bertram, AK, Blanchet, J, Boivin-Rioux, A, Bozem, H, Burkart, J, Chang, RYW, Charette, J, Chaubey, JP. 2019. Overview paper: New insights into aerosol and climate in the Arctic. *Atmospheric Chemistry and Physics* **19**: 2527–2560. DOI: http://dx.doi.org/10.5194/acp-2018-995.

Alcolombri, U, Ben-Dor, S, Feldmesser, E, Levin, Y, Tawfik, DS, Vardi, A. 2015. Identification of the algal dimethyl sulfide-releasing enzyme: A missing link in the marine sulfur cycle. *Science* **348**(6242): 1466–1469. DOI: http://dx.doi.org/10.1126/science.aab1586.

Alou-Font, E, Roy, S, Agustí, S, Gosselin, M. 2016. Cell viability, pigments and photosynthetic performance of Arctic phytoplankton in contrasting ice-covered and open-water conditions during the spring – summer transition. *Marine Ecology Progress Series* **543**: 89–106. DOI: http://dx.doi.org/10.3354/meps11562.

Amiraux, R, Smik, L, Köseoğlu, D, Rontani, JF, Galindo, V, Grondin, PL, Babin, M, Belt, ST. 2019. Temporal evolution of IP25 and other highly branched isoprenoid lipids in sea ice and the underlying water column during an Arctic melting season. *Elementa: Science of the Anthropocene* **7**: 38. DOI: http://dx.doi.org/10.1525/elementa.377.

Andreae, MO, Rosenfeld, D. 2008. Aerosol–cloud–precipitation interactions. Part 1. The nature and sources of cloud-active aerosols. *Earth-Science Reviews* **89**(1–2): 13–41. DOI: http://dx.doi.org/10.1016/j.earscirev.2008.03.001.

Arctic Monitoring & Assessment Programme. 2017. *Snow, Water, Ice and Permafrost in the Arctic (SWIPA) 2017*. Oslo, Norway: Arctic Monitoring & Assessment Programme.

Ardyna, M, Mundy, CJ, Mills, MM, Oziel, L, Lacour, L, Verin, G, Van Dijken, G, Ras, J, Alou-Font, E, Babin, M, Gosselin, M, Tremblay, J-E, Raimbault, P, Assmy, P, Nicolaus, M, Claustre, H, Arrigo, KR. 2020. Environmental drivers of under-ice phytoplankton bloom dynamics in the Arctic Ocean. *Elementa: Science of the Anthropocene* **8**: 30. DOI: http://dx.doi.org/10.1525/elementa.430.

Arrigo, KR, Perovich, DK, Pickart, RS, Brown, ZW, van Dijken, GL, Lowry, KE, Mills, MM, Palmer, MA, Balch, WM, Bates, NR, Benitez-Nelson, CR. 2014. Phytoplankton blooms beneath the sea ice in the Chukchi sea. *Deep Sea Research Part II: Topical Studies in Oceanography* **105**: 105–117. DOI: http://dx.doi.org/10.1016/j.dsr2.2014.03.018.

Assmy, P, Fernández-Méndez, M, Duarte, P, Meyer, A, Randelhoff, A, Mundy, CJ, Olsen, LM, Kauko, HM, Bailey, A, Chierici, M, Cohen, L. 2017. Leads in Arctic pack ice enable early phytoplankton blooms below snow-covered sea ice. *Scientific Reports* **7**: 40850. DOI: http://dx.doi.org/10.1038/srep40850.

Bénard, R, Lizotte, M, Levasseur, M, Scarratt, M, Michaud, S, Starr, M, Tremblay, J-É, Kiene, RP, Kameyama, S. 2021. Impact of anthropogenic pH perturbation on dimethylsulfide cycling: A peek into the microbial black box. *Elementa: Science of the Anthropocene* **9**(1): 00043.

Borcard, D, Gillet, F, Legendre, P. 2011. Canonical ordination, in *Numerical ecology with R*. Springer: 153–225. DOI: http://dx.doi.org/10.1007/978-1-4419-7976-6.

Brean, J, Dall'Osto, M, Simó, R, Shi, Z, Beddows, DCS, Harrison, RM. 2021. Open ocean and coastal new particle formation from sulfuric acid and amines around the Antarctic Peninsula. *Nature Geoscience*. DOI: http://dx.doi.org/10.1038/s41561-021-00751-y.

Brun, P, Vogt, M, Payne, MR, Gruber, N, O'brien, CJ, Buitenhuis, ET, Le Quéré, C, Leblanc, K, Luo, YW. 2015. Ecological niches of open ocean phytoplankton taxa. *Limnology and Oceanography* **60**(3): 1020–1038. DOI: http://dx.doi.org/10.1002/lno.10074.

Burgers, TM, Miller, LA, Thomas, H, Else, BGT, Gosselin, M, Papakyriakou, T. 2017. Surface water pCO_2 variations and sea–air CO_2 fluxes during summer in the Eastern Canadian Arctic. *Journal of Geophysical Research Oceans* **122**(12): 9663–9678. DOI: http://dx.doi.org/10.1002/2017JC013250.

Carpenter, LJ, Archer, SD, Beale, R. 2012. Ocean–atmosphere trace gas exchange. *Chemical Society Reviews* **41**: 6473–6505. DOI: http://dx.doi.org/10.1039/c2cs35121h.

Carslaw, KS, Lee, LA, Reddington, CL, Pringle, KJ, Rap, A, Forster, PM, Mann, GW, Spracklen, DV, Woodhouse, MT, Regayre, LA, Pierce, JR. 2013. Large contribution of natural aerosols to uncertainty in indirect forcing. *Nature* **503**(7474): 67–71. DOI: http://dx.doi.org/10.1038/nature12674.

Caruana, AMN, Malin, G. 2014. The variability in DMSP content and DMSP lyase activity in marine dinoflagellates. *Progress in Oceanography* **120**: 410–424. DOI: http://dx.doi.org/10.1016/j.pocean.2013.10.014.

Castro, SL, Emery, WJ, Wick, GA, Tandy, W. 2017. Submesoscale sea surface temperature variability from UAV and satellite measurements. *Remote Sensing* **9**(11): 1089. DOI: http://dx.doi.org/10.3390/rs9111089.

Cetinić, I, Perry, MJ, Briggs, NT, Kallin, E, D'Asaro, EA, Lee, CM. 2012. Particulate organic carbon and inherent optical properties during 2008 North Atlantic bloom experiment. *Journal of Geophysical Research Oceans* **117**(6). DOI: http://dx.doi.org/10.1029/2011JC007771.

Charlson, RJ, Lovelock, JE, Andreae, MO, Warren, SG. 1987. Oceanic phytoplankton, atmospheric sulphur, cloud albedo and climate. *Nature* **326**: 655–661. DOI: http://dx.doi.org/10.1038/326655a0.

Collins, DB, Burkart, J, Chang, RY-W, Lizotte, M, Boivin-Rioux, A, Blais, M, Mungall, EL, Boyer, M, Irish, VE, Massé, G, Kunkel, D. 2017. Frequent ultrafine particle formation and growth in the Canadian Arctic marine environment. *Atmospheric Chemistry and Physics* **17**: 13119–13138. DOI: http://dx.doi.org/10.5194/acp-2017-411.

Cota, GF, Smith WO, Mitchell, BG. 1994. Photosynthesis of *Phaeocystis* in the Greenland Sea. *Limnology and Oceanography* **39**(4): 948–953. DOI: http://dx.doi.org/10.4319/lo.1994.39.4.0948

Coupel, P, Matsuoka, A, Ruiz-Pino, D, Gosselin, M, Marie, D, Tremblay, JE, Babin, M. 2015. Pigment signatures of phytoplankton communities in the Beaufort Sea. *Biogeosciences* **12**(4): 991–1006. DOI: http://dx.doi.org/10.5194/bg-12-991-2015.

Croft, B, Martin, R V, Leaitch, WR, Tunved, P, Breider, TJ, Andrea, SDD, Pierce JR. 2016. Processes controlling the annual cycle of Arctic aerosol number and size distributions. *Atmospheric Chemistry and Physics* **16**(6): 3665–3682. DOI: http://dx.doi.org/10.5194/acp-16-3665-2016.

Curson, A, Liu, J, Bermejo Martínez, A, Green, RT, Chan, Y, Carrión, O, Williams, BT, Zhang, S-H, Yang, G-P, Page, PCB, Zhang, X-H, Todd, JD. 2017. Dimethylsulfoniopropionate biosynthesis in marine bacteria and identification of the key gene in this process. *Nature Microbiology* **2**: 17009. DOI: https://doi.org/10.1038/nmicrobiol.2017.9.

Curson, ARJ, Todd, JD, Sullivan, MJ, Johnston, AWB. 2011. Catabolism of dimethylsulphoniopropionate: Microorganisms, enzymes and genes. *Nature reviews Microbiology* **9**(12): 849–859. DOI: http://dx.doi.org/10.1038/nrmicro2653.

Dall'Osto, M, Beddows, DCS, Tunved, P, Krejci, R, Ström, J, Hansson, H-C, Yoon, YJ, Park, K-T, Becagli, S, Udisti, R, Onasch, T. 2017. Arctic sea ice melt leads to atmospheric new particle formation. *Scientific Reports* **7**(1): 3318. DOI: http://dx.doi.org/10.1038/s41598-017-03328-1.

Dawson, ML, Varner, ME, Perraud, V, Ezell, MJ, Gerber, RB, Finlayson-Pitts, BJ. 2012. Simplified mechanism for new particle formation from methanesulfonic acid, amines, and water via experiments and ab initio calculations. *Proceedings of the National Academy of Sciences* **109**(46): 18719–18724. DOI: http://dx.doi.org/10.1073/pnas.1211878109.

del Valle, D, Kieber, DJ, Kiene, RP. 2007. Depth-dependent fate of biologically-consumed dimethylsulfide in the Sargasso Sea. *Marine Chemistry* **103**(1–2): 197–208. DOI: http://dx.doi.org/10.1016/j.marchem.2006.07.005.

del Valle, D, Kieber, DJ, Toole, DA, Brinkley, J, Kiene, RP. 2009. Biological consumption of dimethylsulfide (DMS) and its importance in DMS dynamics in the Ross Sea, Antarctica. *Limnology and Oceanography* **54**(3): 785–798.

Eilertsen, HC, Taasen, JP, Wesiawski, JM. 1989. Phytoplankton studies in the fjords of West Spitzbergen: Physical environment and production in spring and summer. *Journal of Plankton Research* **11**(6): 1245–1260. DOI: http://dx.doi.org/10.1093/plankt/11.6.1245.

Engel, A, Piontek, J, Metfies, K, Endres, S, Sprong, P, Peeken, I, Gäbler-Schwarz, S, Nöthig, EM. 2017. Inter-annual variability of transparent exopolymer particles in the Arctic Ocean reveals high sensitivity to ecosystem changes. *Scientific Reports* **7**(1): 1–9. DOI: http://dx.doi.org/10.1038/s41598-017-04106-9.

Fernández-Gómez, B, Richter, M, Schüler, M, Pinhassi, J, Acinas, SG, González, JM, Pedrós-Alió, C. 2013. Ecology of marine Bacteroidetes: A comparative genomics approach. *ISME Journal* **7**(5): 1026–1037. DOI: http://dx.doi.org/10.1038/ismej.2012.169.

Fernández-Méndez, M, Olsen, LM, Kauko, HM, Meyer, A, Rösel, A, Merkouriadi, I, Mundy, CJ, Ehn, JK, Johansson, AM, Wagner, PM, Ervik, Å. 2018. Algal hot spots in a changing Arctic Ocean: Sea-ice ridges and the snow-ice interface. *Frontiers in Marine Science* **5**: 75. DOI: http://dx.doi.org/10.3389/fmars.2018.00075.

Gabric, A, Matrai, P, Jones, GM, Middleton, J. 2018. The nexus between sea ice and polar emissions of marine biogenic aerosols. *Bulletin of the American Meteorological Society* **99**(1): 61–82. DOI: http://dx.doi.org/10.1175/BAMS-D-16-.

Galí, M, Devred, E, Babin, M, Levasseur, M. 2019. Decadal increase in Arctic dimethylsulfide emission. *Proceedings of the National Academy of Sciences* **116**(39): 19311–19317. DOI: http://dx.doi.org/10.1073/pnas.1904378116.

Galí, M, Kieber, DJ, Romera-Castillo, C, Kinsey, JD, Devred, E, Pérez, GL, Westby, GR, Marrasé, C, Babin, M, Levasseur, M, Duarte, CM. 2016. CDOM sources and photobleaching control quantum yields for oceanic DMS photolysis. *Environmental Science & Technology* **50**: 13361–13370. DOI: http://dx.doi.org/10.1021/acs.est.6b04278.

Galí, M, Levasseur, M, Devred, E, Simó, R, Babin, M. 2018. Sea-surface dimethylsulfide (DMS) concentration from satellite data at global and regional scales. *Biogeosciences* **15**: 3497–3519. DOI: http://dx.doi.org/10.5194/bg-15-3497-2018.

Galí, M, Ruiz-González, C, Lefort, T, Gasol, JM, Cardelús, C, Romera-Castillo, C, Simó, R. 2013. Spectral irradiance dependence of sunlight effects on plankton dimethylsulfide production. *Limnology and Oceanography* **58**(2): 489–504. DOI: http://dx.doi.org/10.4319/lo.2013.58.2.0489.

Galí, M, Simó, R. 2010. Occurrence and cycling of dimethylated sulfur compounds in the Arctic during summer receding of the ice edge. *Marine Chemistry* **122**: 105–117. DOI: http://dx.doi.org/10.1016/j.marchem.2010.07.003.

Galí, M, Simó, R. 2015. A meta-analysis of oceanic DMS and DMSP cycling processes: Disentangling the summer paradox. *Global Biogeochemical Cycles* **29**: 496–515. DOI: http://dx.doi.org/10.1002/2014GB004940.

Galindo, V, Levasseur, M, Mundy, CJ, Gosselin, M, Scarratt, M, Papakyriakou, T, Stefels, J, Gale, MA, Tremblay, J-É, Lizotte, M. 2016. Contrasted sensitivity of DMSP production to high light exposure in two Arctic under-ice blooms. *Journal of Experimental Marine Biology and Ecology* **475**: 38–48. DOI: http://dx.doi.org/10.1016/j.jembe.2015.11.009.

Galindo, V, Levasseur, M, Mundy, CJ, Gosselin, M, Tremblay, J-É, Scarratt, MG, Gratton, Y, Papakiriakou, T, Poulin, M, Lizotte, M. 2014. Biological and physical processes influencing sea ice, under-ice algae, and dimethylsulfoniopropionate during spring in the Canadian archipelago. *Journal of Geophysical Research Oceans* **119**: 3746–3766. DOI: http://dx.doi.org/10.1002/2013JC009497.

Galindo, V, Levasseur, M, Scarratt, M, Mundy, C, Gosselin, M, Kiene, R, Gourdal, M, Lizotte, M. 2015. Under-ice microbial dimethylsulfoniopropionate metabolism during the melt period in the Canadian Arctic Archipelago. *Marine Ecology Progress Series* **524**: 39–53. DOI: http://dx.doi.org/10.3354/meps11144.

Gasol, JM, del Giorgio, PA. 2000. Using flow cytometry for counting natural planktonic bacteria and understanding the structure of planktonic bacterial communities. *Scientia Marina* **64**(2): 197–224. DOI: http://dx.doi.org/10.3989/scimar.2000.64n2197.

Ghahremaninezhad, R, Gong, W, Galí, M, Norman, A-L, Beagley, SR, Akingunola, A, Zheng, Q, Lupu, A, Lizotte, M, Levasseur, M, Leaitch, WR. 2019. Dimethyl sulfide and its role in aerosol formation and growth in the Arctic summer - a modelling study. *Atmospheric Chemistry and Physics* **19**(23): 14455–14476. DOI: http://dx.doi.org/10.5194/acp-19-14455-2019.

Gourdal, M, Lizotte, M, Massé, G, Gosselin, M, Scarratt, M, Levasseur, M. 2018. Dimethylsulfide dynamics in first-year sea ice melt ponds in the Canadian Arctic Archipelago. *Biogeosciences* **15**: 3169–3188. DOI: http://dx.doi.org/10.5194/bg-2017-432.

Grondin, PL. 2019. *Microalgae species succession and its drivers during under-ice spring blooms in the Arctic Ocean* [MSc thesis]. Laval University.

Hansen, E, Eilertsen, HC. 2007. Do the polyunsaturated aldehydes produced by *Phaeocystis pouchetii* (Hariot) Lagerheim influence diatom growth during the spring bloom in Northern Norway? *Journal of Plankton Research* **29**(1): 87–96. DOI: http://dx.doi.org/10.1093/plankt/fbl065.

Hayashida, H, Carnat G, Galí M, Monahan AH, Mortenson E, Sou T, Steiner NS. 2020. Spatio-temporal variability in modelled bottom-ice and sea-surface dimethylsulfide concentrations and fluxes in the Arctic during 1979–2015. *Global Biogeochemical Cycles* **34**(10): e2019GB006456. DOI: http://dx.doi.org/10.1029/2019GB006456.

Heintzenberg, J, Leck C, Tunved P. 2015. Potential source regions and processes of aerosol in the summer Arctic. *Atmospheric Chemistry and Physics* **15**(11): 6487–6502. DOI: http://dx.doi.org/10.5194/acp-15-6487-2015.

Heintzenberg, J, Tunved P, Galí M, Leck C. 2017. New particle formation in the Svalbard region 2006–2015. *Atmospheric Chemistry and Physics* **17**: 6153–6175. DOI: http://dx.doi.org/10.5194/acp-2016-1073.

Hodshire, AL, Campuzano-Jost, P, Kodros, JK, Croft, B, Nault, BA, Schroder, JC, Jimenez, JL, Pierce, JR. 2019. The potential role of methanesulfonic acid (MSA) in aerosol formation and growth and the associated radiative forcings. *Atmospheric Chemistry and Physics* **19**(5): 3137–3160. DOI: http://dx.doi.org/10.5194/acp-19-3137-2019.

Hopkins, FE, Nightingale PD, Stephens JA, Moore CM, Richier S, Cripps GL, Archer SD. 2020. A meta-analysis of microcosm experiments shows that dimethyl sulfide (DMS) production in polar waters is insensitive to ocean acidification. *Biogeosciences* **17**(1): 163–186. DOI: http://dx.doi.org/10.5194/bg-17-163-2020.

Hsu, SA, Meindl, EA, Gilhousen, DB. 1994. Determining the power-law wind-profile exponent under near-neutral stability conditions at sea. *Journal of Applied Meteorology* **33**(6): 757–765. DOI: http://dx.doi.org/10.16309/j.cnki.issn.1007-1776.2003.03.004.

Hussherr, R, Levasseur, M, Lizotte, M, Tremblay, J-É, Mol, J, Thomas, H, Gosselin, M, Starr, M, Miller, LA, Jarniková, T, Schuback, N, Mucci, A. 2017. Impact of ocean acidification on Arctic phytoplankton blooms and dimethyl sulfide concentration under simulated ice-free and under-ice conditions. *Biogeosciences* **14**(9): 2407–2427.

Inness, A, Chabrillat, S, Flemming, J, Huijnen, V, Langenrock, B, Nicolas J, Polichtchouk, I, Razinger, M. 2020. Exceptionally low Arctic stratospheric ozone in spring 2020 as seen in the CAMS reanalysis. *Journal of Geophysical Research-Atmospheres* **125**(23): e2020JD033563. DOI: http://dx.doi.org/10.1029/2020JD033563.

Intergovernmental Panel on Climate Change. 2019. IPCC Special Report on the Ocean and Cryosphere in a Changing Climate [H.-O. Pörtner, D.C. Roberts, V. Masson-Delmotte, P. Zhai, M. Tignor, E. Poloczanska, K. Mintenbeck, A. Alegría, M. Nicolai, A. Okem, J. Petzold, B. Rama, N.M. Weyer (eds.)]. Available at https://www.ipcc.ch/srocc/.

Jarníková, T, Dacey, JW, Lizotte, M, Levasseur, M, Tortell, PD. 2018. The distribution of methylated sulfur compounds, DMS and DMSP, in Canadian Subarctic and Arctic waters during summer 2015. *Biogeosciences* **15**: 2449–2465. DOI: http://dx.doi.org/10.5194/bg-15-2449-2018.

Jeffrey, SW, Wright, SW, Zapata, M. 2012. Microalgal classes and their signature pigments, in Roy, S, Llewellyn, CA, Egeland, ES, Johnsen, G eds., *Phytoplankton pigments: Characterization, chemotaxonomy and applications in oceanography*. Cambridge University Press: 3–77. DOI: http://dx.doi.org/10.1017/cbo9780511732263.004.

Kameyama, S, Otomaru, M, McMinn, A, Suzuki, K. 2020. Ice melting can change DMSP production and photosynthetic activity of the haptophyte phaeocystis antarctica. *Journal of Phycology* **56**(3): 761–774.

Keller, MD. 1989. Dimethyl sulfide production in marine phytoplankton, in Saltzman, ES, Cooper, WJ eds., *Biogenic sulfur in the environment*. New York, NY (ACS Symposium series): 167–182. Available at https://pubs.acs.org/doi/abs/10.1021/bk-1989-0393.ch011.

Kieber, DJ, Jiao, J, Kiene, RP, Bates, TS. 1996. Impact of dimethylsulfide photochemistry on methyl sulfur cycling in the equatorial Pacific Ocean. *Journal of Geophysical Research* **101**(C2): 3715–3722. DOI: http://dx.doi.org/10.1029/95JC03624.

Kiene, RP, Bates, TS. 1990. Biological removal of dimethyl sulphide from sea water. *Nature* **345**: 702–705. DOI: http://dx.doi.org/10.1038/345702a0.

Kiene, RP, Linn, L, Bruton, J. 2000. New and important roles for DMSP in marine microbial communities. *Journal of Sea Research* **43**: 209–224. DOI: http://dx.doi.org/10.1016/S1385-1101(00)00023-X.

Kiene, RP, Linn, LJ. 2000. The fate of dissolved dimethylsulfoniopropionate (DMSP) in seawater: tracer studies using 35S-DMSP. *Geochimica et Cosmochimica Acta* **64**(16): 2797–2810. DOI: http://dx.doi.org/10.1016/S0016-7037(00)00399-9.

Kiene, RP, Slezak, D. 2006. Low dissolved DMSP concentrations in seawater revealed by small volume gravity filtration and dialysis sampling. *Limnology and Oceanography: Methods* **4**: 80–95.

Kinsey, JD, Kieber, DJ. 2016. Microwave preservation method for DMSP, DMSO, and acrylate in unfiltered seawater and phytoplankton culture samples. *Limnology and Oceanography Methods* **14**(3): 196–209. DOI: http://dx.doi.org/10.1002/lom3.10081.

Kinsey, JD, Kieber, DJ, Neale, PJ. 2016. Effects of iron limitation and UV radiation on *Phaeocystis antarctica* growth and dimethylsulfoniopropionate, dimethylsulfoxide and acrylate concentrations. *Environmental Chemistry* **13**(2): 195–211. DOI: http://dx.doi.org/10.1071/EN14275.

Koroleff, F, Hansen HP. 1999. Determination of nutrients, in Grasshoff, K, Kremling, K, Ehrhardt, M eds., *Methods of seawater analysis*. New York, NY: Wiley: 159–228. DOI: http://dx.doi.org/10.1002/9783527613984.ch10.

Krawczyk, DW, Meire, L, Lopes, C, Juul-Pedersen, T, Mortensen, J, Li, CL, Krogh, T. 2018. Seasonal succession, distribution, and diversity of planktonic protists in relation to hydrography of the Godthåbsfjord system (SW Greenland). *Polar Biology* **41**(10): 2033–2052. DOI: http://dx.doi.org/10.1007/s00300-018-2343-0.

Kubiszyn, AM, Wiktor, JM, Wiktor, JM, Griffiths, C, Kristiansen, S, Gabrielsen, TM. 2017. The annual planktonic protist community structure in an ice-free high Arctic fjord (Adventfjorden, West Spitsbergen). *Journal of Marine Systems* **169**: 61–72. DOI: http://dx.doi.org/10.1016/j.jmarsys.2017.01.013.

Lacour, T, Larivière, J, Babin, M. 2017. Growth, Chl *a* content, photosynthesis, and elemental composition in

polar and temperate microalgae. *Limnology and Oceanography* ***62***(1): 43–58. DOI: http://dx.doi.org/10.1002/lno.10369.

Lafond, A, Leblanc, K, Quéguiner, B, Moriceau, B, Leynaert, A, Cornet, V, Legras, J, Ras, J, Parenteau, M. 2019. Late spring bloom development of pelagic diatoms in Baffin Bay. *Elementa: Science of the Anthropocene* **7**(44). DOI: http://dx.doi.org/10.1525/elementa.382.

Laliberté, J, Bélanger, S, Frouin, R. 2016. Evaluation of satellite-based algorithms to estimate photosynthetically available radiation (PAR) reaching the ocean surface at high northern latitudes. *Remote Sensing of Environment* **184**: 199–211. DOI: http://dx.doi.org/10.1016/j.rse.2016.06.014.

Lana, A, Bell, TG, Simó, R, Vallina, SM, Ballabrera-Poy, J, Kettle, AJ, Dachs, J, Bopp, L, Saltzman, ES, Stefels, J, Johnson, JE. 2011. An updated climatology of surface dimethlysulfide concentrations and emission fluxes in the global ocean. *Global Biogeochemical Cycles* **25**: GB1004. DOI: http://dx.doi.org/10.1029/2010GB003850.

Land, PE, Shutler, JD, Bell, TG, Yang, M. 2014. Exploiting satellite earth observation to quantify current global oceanic DMS flux and its future climate sensitivity. *Journal of Geophysical Research Oceans* **119**(11): 7725–7740. DOI: http://dx.doi.org/10.1002/2014JC010104.

Landa, M, Burns, AS, Durham, BP, Esson, K, Nowinski, B, Sharma, S, Vorobev, A, Nielsen T, Kiene, RP, Moran, MA. 2019. Sulfur metabolites that facilitate oceanic phytoplankton–bacteria carbon flux. *ISME Journal* **13**: 2536–2550. DOI: http://dx.doi.org/10.1038/s41396-019-0455-3,2019.

Lasternas, S, Agustí, S. 2010. Phytoplankton community structure during the record Arctic ice-melting of summer 2007. *Polar Biology* **33**(12): 1709–1717. DOI: http://dx.doi.org/10.1007/s00300-010-0877-x.

Leaitch, WR, Sharma, S, Huang, L, Toom-Sauntry, D, Chivulescu, A, Macdonald, AM, von Salzen, K, Pierce, JR, Bertram, AK, Schroder, JC, Shantz, NC, Chang, RY-W, Norman, A-L. 2013. Dimethyl sulfide control of the clean summertime Arctic aerosol and cloud. *Elementa: Science of the Anthropocene* **1**: 000017. DOI: http://dx.doi.org/10.12952/journal.elementa.000017.

Le Clainche, Y, Levasseur, M, Vézina, A, Bouillon, R-C, Merzouk, A, Michaud, S, Scarratt, M, Wong, C, Rivkin, RB, Boyd, PW, Harrison, PJ. 2006. Modeling analysis of the effect of iron enrichment on dimethyl sulfide dynamics in the NE Pacific (SERIES experiment). *Journal of Geophysical Research* **111**(C1): 1–15. DOI: http://dx.doi.org/10.1029/2005JC002947.

Letelier, RM, Karl, DM, Abbott, MR, Bidigare, RR. 2004. Light driven seasonal patterns of chlorophyll and nitrate in the lower euphotic zone of the North Pacific Subtropical Gyre. *Limnology and Oceanography* **49**(2): 508–519. DOI: http://dx.doi.org/10.4319/lo.2004.49.2.0508.

Leu, E, Mundy, CJ, Assmy, P, Campbell, K, Gabrielsen, TM, Gosselin, M, Juul-Pedersen, T, Gradinger, R. 2015. Arctic spring awakening–Steering principles behind the phenology of vernal ice algal blooms. *Progress in Oceanography* **139**: 151–170. DOI: http://dx.doi.org/10.1016/j.pocean.2015.07.012.

Levasseur, M. 2013. Impact of Arctic meltdown on the microbial cycling of sulphur. *Nature Geoscience* **6**(9): 691–700. DOI: http://dx.doi.org/10.1038/ngeo1910.

Levine, NM, Varaljay, VA, Toole, DA, Dacey, JWH, Doney, SC, Moran, MA. 2012. Environmental, biochemical and genetic drivers of DMSP degradation and DMS production in the Sargasso Sea. *Environmental Microbiology* **14**(5): 1210–1223. DOI: http://dx.doi.org/10.1111/j.1462-2920.2012.02700.x.

Li, C-Y, Wang, X-J, Chen, X-L, Sheng, Q, Zhang, S, Wang, P, Quareshy, M, Rihtman, B, Shao, X, Gao, C, Li, F, Li, S. 2020. Novel enzyme for dimethyl sulfide-releasing in bacteria reveals a missing route in the marine sulfur cycle. *bioRxiv preprint*. DOI: http://dx.doi.org/10.1101/2020.10.29.360743.

Lidbury, I, Kröber, E, Zhang, Z, Zhu, Y, Murrell, JC, Chen, Y, Schäfer, H. 2016. A mechanism for bacterial transformations of DMS to DMSO: A missing link in the marine organic sulfur cycle. *Environmental Microbiology* **18**(8): 2754–2766. DOI: http://dx.doi.org/10.1111/1462-2920.13354.

Lizotte, M, Levasseur, M, Galindo, V, Gourdal, M, Gosselin, M, Tremblay, JE, Blais, M, Charette, J, Hussherr, R. 2020. Phytoplankton and dimethylsulfide dynamics at two contrasting Arctic ice edges. *Biogeosciences* **17**: 1557–1581. DOI: http://dx.doi.org/10.5194/bg-17-1557-2020.

Lizotte, M, Levasseur, M, Scarratt, M, Michaud, S, Merzouk, A, Gosselin, M, Pommier, J. 2008. Fate of dimethylsulfoniopropionate (DMSP) during the decline of the northwest Atlantic Ocean spring diatom bloom. Aquatic Microbial Ecology **52**(August): 159–173. DOI: http://dx.doi.org/10.3354/ame01232.

Loisel, H, Morel, A. 1998. Light scattering and chlorophyll concentration in case 1 waters: A reexamination. *Limnology and Oceanography* **43**(5), 847–858. DOI: http://dx.doi.org/10.4319/lo.1998.43.5.0847.

Long, JD, Smalley, GW, Barsby, T, Anderson, JT, Hay, ME. 2007. Chemical cues induce consumer-specific defenses in a bloom-forming marine phytoplankton. *Proceedings of the National Academy of Sciences USA* **104**(25): 10512–7. DOI: http://dx.doi.org/10.1073/pnas.0611600104.

Mahmood, R, von Salzen, K, Norman, A-L, Galí, M, Levasseur, M. 2019. Sensitivity of Arctic sulfate aerosol and clouds to changes in future surface seawater dimethylsulfide concentrations. *Atmospheric Chemistry and Physics* **19**: 6419–6435. DOI: http://dx.doi.org/10.5194/acp-2018-876.

Malin, G, Wilson, WH, Bratbak, G, Liss, PS, Mann, NH. 1998. Elevated production of dimethylsulfide resulting from viral infection of cultures of *Phaeocystis pouchetii*. *Limnology and Oceanography* **43**(6): 1389–1393. DOI: http://dx.doi.org/10.4319/lo.1998.43.6.1389.

Manucharyan, GE, Thompson, AF. 2017. Submesoscale sea ice-ocean interactions in marginal ice zones. *Journal of Geophysical Research Oceans* **122**(12): 9455–9475. DOI: http://dx.doi.org/10.1002/2017JC012895.

Marie, D, Brussaard, C, Partensky, F, Vaulot, D. 1999. Flow cytometric analysis of phytoplankton, bacteria and viruses, in Robinson, JP ed., Vol. 11.11. *Current protocols in cytometry*. New York, NY: John Wiley and Sons: 1–15.

Matrai, P, Vernet, M, Wassmann, P. 2007. Relating temporal and spatial patterns of DMSP in the Barents Sea to phytoplankton biomass and productivity. *Journal of Marine Systems* **67**(1-2): 83–101. DOI: http://dx.doi.org/1016/j.jmarsys.2006.10.001.

Matrai, PA, Vernet, M. 1997. Dynamics of the vernal bloom in the marginal ice zone of the Barents Sea: Dimethyl sulfide and dimethylsulfoniopropionate budgets. *Journal of Geophysical Research: Oceans* **102**(C10): 22965–22979.

Matrai, PA, Vernet, M, Hood, R, Jennings, A, Brody, E, Saemundsdóttir, S. 1995. Light-dependence of carbon and sulfur production by polar clones of the genus *Phaeocystis*. *Marine Biology* **124**(1): 157–167. DOI: http://dx.doi.org/10.1007/BF00349157.

Mauritsen, T, Sedlar, J, Tjernström, M, Leck, C, Martin, M, Shupe, M, Sjogren, S, Sierau, B, Persson, POG, Brooks, IM, Swietlicki, E. 2011. An Arctic CCN-limited cloud-aerosol regime. *Atmospheric Chemistry and Physics* **11**: 165–173. DOI: http://dx.doi.org/10.5194/acp-11-165-2011.

McParland, EL, Levine, NM. 2019. The role of differential DMSP production and community composition in predicting variability of global surface DMSP concentrations. *Limnology and Oceanography* **64**(2): 757–773. DOI: http://dx.doi.org/10.1002/lno.11076.

McPhee, M. 2008. *Air-ice-ocean interaction: Turbulent ocean boundary layer exchange processes*. New York, NY: Springer. DOI: http://dx.doi.org/10.1007/978-0-387-78335-2.

Menden-Deuer, S, Lessard, EJ. 2000. Carbon to volume relationships for dinoflagellates, diatoms, and other protist plankton. *Limnology and Oceanography* **45**(3): 569–579. DOI: http://dx.doi.org/10.4319/lo.2000.45.3.0569.

Metfies, K, Von Appen, WJ, Kilias, E, Nicolaus, A, Nöthig, EM. 2016. Biogeography and photosynthetic biomass of Arctic marine pico-eukaroytes during summer of the record sea ice minimum 2012. *PLoS One* **11**(2): 1–20. DOI: http://dx.doi.org/10.1371/journal.pone.0148512.

Mungall, EL, Croft, B, Lizotte, M, Thomas, JL, Murphy, JG, Levasseur, M, Martin, RV, Wentzell, JJB, Liggio, J, Abbatt, JPD. 2016. Dimethyl sulfide in the summertime Arctic atmosphere: measurements and source sensitivity simulations. *Atmospheric Chemistry and Physics* **16**: 6665–6680. DOI: http://dx.doi.org/10.5194/acp-16-6665-2016.

Oksanen, J, Blanchet, FG, Friendly, M, Kindt, R, Legendre, P, McGlinn, D, Minchin, PR, O'Hara RB, Simpson, GL, Solymos, P, Stevens, MHM, Szoecs, E, Wagner, H. 2019. vegan: Community Ecology Package. R package version 2.5-6. Available at https://CRAN.R-project.org/package=vegan.

Olson, RJ, Sosik, HM. 2007. A submersible imaging-in-flow instrument to analyze nano- and microplankton: Imaging FlowCytobot. *Limnology and Oceanography Meth* **5**: 195–203. DOI: http://dx.doi.org/10.4319/lom.2007.5.195.

Orellana, MV, Matrai, PA, Janer, M, Rauschenberg, CD. 2011. Dimethylsulfoniopropionate storage in *Phaeocystis* (Prymnesiophyceae) secretory vesicles. *Journal of Phycology* **47**(1): 112–117. DOI: http://dx.doi.org/10.1111/j.1529-8817.2010.00936.x.

Orkney, A, Platt, T, Narayanaswamy, BE, Kostakis, I, Bouman, HA. 2020. Bio-optical evidence for increasing *Phaeocystis* dominance in the Barents Sea. *Philosophical Transactions of the Royal Society A* **378**(2181): 20190357. DOI: http://dx.doi.org/10.1098/rsta.2019.0357.

Park, K, Kim, I, Choi, JO, Lee, Y, Jung, J, Ha, SY, Kim, JH, Zhang, M. 2019. Unexpectedly high dimethyl sulfide concentration in high-latitude Arctic sea ice melt ponds. *Environmental Science: Processes & Impacts* **21**(10): 1642–1649. DOI: http://dx.doi.org/10.1039/c9em00195f.

Perrette, M, Yool, A, Quartly, GD, Popova, EE. 2011. Near-ubiquity of ice-edge blooms in the Arctic. *Biogeosciences* **8**(2): 515–524. DOI: http://dx.doi.org/10.5194/bg-8-515-2011.

Quinn, PK, Bates, TS. 2011. The case against climate regulation via oceanic phytoplankton sulphur emissions. *Nature* **480**: 51–56. DOI: http://dx.doi.org/10.1038/nature10580.

Randelhoff, A, Fer, I, Sundfjord, A. 2017. Turbulent upper-ocean mixing affected by meltwater layers during Arctic summer. *Journal of Physical Oceanography* **47**(4): 835–853. DOI: http://dx.doi.org/10.1175/JPO-D-16-0200.1.

Randelhoff, A, Holding, J, Janout, M, Sejr, MK, Babin, M, Tremblay, JÉ, Alkire, MB. 2020. Pan-Arctic ocean primary production constrained by turbulent nitrate fluxes. *Frontiers in Marine Science* **7**: 150. DOI: http://dx.doi.org/10.3389/fmars.2020.00150.

Randelhoff, A, Oziel, L, Massicotte, P, Bécu, G, Galí, M, Lacour, L, Dumont, D, Vladoiu, A, Marec, C, Bruyant, F, Houssais, MN. 2019. The evolution of light and vertical mixing across a phytoplankton ice-edge bloom. *Elementa: Science of the Anthropocene* **7**(1). DOI: http://dx.doi.org/10.1525/elementa.357.

Ras, J, Claustre, H, Uitz, J. 2008. Spatial variability of phytoplankton pigment distributions in the Subtropical South Pacific Ocean: Comparison between

in situ and predicted data. *Biogeosciences* **5**(2): 353–369. DOI: http://dx.doi.org/10.5194/bg-5-353-2008.

R Core Team. 2017. *R: A language and environment for statistical computing*. Vienna, Austria: R Foundation for Statistical Computing. Available at https://www.R-project.org/.

Reigstad, M, Wassmann, P. 2007. Does *Phaeocystis* spp. contribute significantly to vertical export of organic carbon? *Biogeochemistry* **83**(1–3): 217–234. DOI: http://dx.doi.org/10.1007/s10533-007-9093-3.

Rellinger, AN, Kiene, RP, del Valle, DA, Kieber, DJ, Slezak, D, Harada, H, Bisgrove, J, Brinkley, J. 2009. Occurrence and turnover of DMSP and DMS in deep waters of the Ross Sea, Antarctica. *Deep Sea Research Part I* **56**(5): 686–702. DOI: http://dx.doi.org/10.1016/j.dsr.2008.12.010.

Renaut, S, Devred, E, Babin, M. 2018. Northward expansion and intensification of phytoplankton growth during the early ice-free season in Arctic. *Geophysical Research Letters* **45**: 10,590–10,598. DOI: http://dx.doi.org/10.1029/2018GL078995.

Ricchiazzi, P, Yang, S, Gautier, C, Sowle, D. 1998. SBDART: A research and teaching software tool for plane-parallel radiative transfer in the Earth's atmosphere. *Bulletin of the American Meteorological Society* **79**(10): 2101–2114. DOI: http://dx.doi.org/10.1175/1520-0477(1998)079<2101:SARATS>2.0.CO;2.

Rowan, KS. 1989. The carotenoids, in *Photosynthetic pigments of algae*. New York, NY: Cambridge University Press: 112–165. Available at https://www.cambridge.org/es/academic/subjects/life-sciences/plant-science/photosynthetic-pigments-algae?format=PB.

Ruiz-González, C, Galí, M, Sintes, E, Herndl, GJ, Gasol, JM, Simó, R. 2012. Sunlight effects on the osmotrophic uptake of DMSP-sulfur and leucine by polar phytoplankton. *PLoS One* **7**(9): e45545. DOI: http://dx.doi.org/10.1371/journal.pone.0045545.

Saint-Béat, B, Fath, BD, Aubry, C, Colombet, J, Dinasquet, J, Fortier, L, Galindo, V, Grondin, PL, Joux, F, Lalande, C, LeBlanc, M. 2020. Contrasting pelagic ecosystem functioning in eastern and western Baffin Bay revealed by trophic network modeling. *Elementa: Science of the Anthropocene* **8**(1): 1–24. DOI: http://dx.doi.org/10.1525/elementa.397

Sanderson, MP, Bronk, DA, Nejstgaard, JC, Verity, PG, Sazhin, AF, Frischer, ME. 2008. Phytoplankton and bacterial uptake of inorganic and organic nitrogen during an induced bloom of *Phaeocystis pouchetii*. *Aquatic Microbial Ecology* **51**(2): 153–168. DOI: http://dx.doi.org/10.3354/ame01178.

Scarratt, M, Cantin, G, Levasseur, M, Michaud, S. 2000. Particle size-fractionated kinetics of DMS production: Where does DMSP cleavage occur at the microscale. *Journal of Sea Research* **43**: 245–252. DOI: http://dx.doi.org/10.1016/S1385-1101(00)00019-8.

Schanke, NL, Bolinesi, F, Mangoni, O, Katlein, C, Anhaus, P, Hoppmann, M, Lee, PA, DiTullio, GR. 2020. Biogeochemical and ecological variability during the late summer–early autumn transition at an ice-floe drift station in the Central Arctic Ocean. *Limnology and Oceanography* **66**:.S363–S382. DOI: http://dx.doi.org/10.1002/lno.11676.

Schoemann, V, Becquevort, S, Stefels, J, Rousseau, V, Lancelot, C. 2005. *Phaeocystis* blooms in the global ocean and their controlling mechanisms: A review. *Journal of Sea Research* **53**(1–2): 43–66. DOI: http://dx.doi.org/10.1016/j.seares.2004.01.008.

Selz, V, Lowry, KE, Lewis, KM, Joy-Warren, HL, Van De Poll, W, Nirmel, S, Tong, A, Arrigo, KR. 2018. Distribution of *Phaeocystis antarctica*-dominated sea ice algal communities and their potential to seed phytoplankton across the western Antarctic Peninsula in spring. *Marine Ecology Progress Series* **586**: 91–112. DOI: http://dx.doi.org/10.3354/meps12367.

Serreze, MC, Barry, RG. 2011. Processes and impacts of Arctic amplification: A research synthesis. *Global and Planetary Change* **77**: 85–96. DOI: http://dx.doi.org/10.1016/j.gloplacha.2011.03.004.

Sheehan, CE, Petrou, K. 2019. Dimethylated sulfur production in batch cultures of Southern Ocean phytoplankton. *Biogeochemistry* **147**(1): 53–69. DOI: http://dx.doi.org/10.1007/s10533-019-00628-8.

Sherr, EB, Sherr, BF, Wheeler, PA, Thompson, K. 2003. Temporal and spatial variation in stocks of autotrophic and heterotrophic microbes in the upper water column of the central Arctic Ocean. *Deep-Sea Research Part I: Oceanographic Research* **50**: 557–571. DOI: http://dx.doi.org/10.1016/S0967-0637(03)00031-1.

Simó, R. 2001. Production of atmospheric sulfur by oceanic plankton: Biogeochemical, ecological and evolutionary links. *Trends in Ecology & Evolution* **16**(6): 287–294.

Simó, R. 2011. The role of marine microbiota in short-term climate regulation, in Duarte, CM ed., *The role of marine biota in the functioning of the biosphere*. Bilbao, Spain: Fundación BBVA: 107–130.

Simó, R, Saló, V, Almeda, R, Movilla, J, Trepat, I, Saiz, E, Calbet, A. 2018. The quantitative role of microzooplankton grazing in dimethylsulfide (DMS) production in the NW Mediterranean. *Biogeochemistry* **141**: 125–142. DOI: http://dx.doi.org/10.1007/s10533-018-0506-2.

Simo-Matchim, A-G, Gosselin, M, Poulin, M, Ardyna, M, Lessard, S. 2017. Summer and fall distribution of phytoplankton in relation to environmental variables in Labrador fjords, northeastern Canada, with special emphasis on *Phaeocystis pouchetii*. *Marine Ecology Progress Series* **572**: 19–42. DOI: http://dx.doi.org/10.3354/meps12125.

Simon, M, Azam, F. 1989. Protein content and protein synthesis rates of planktonic marine bacteria. *Marine Ecology Progress Series* **51**: 201–213.

Six, KD, Kloster, S, Ilyina, T, Archer, SD, Zhang, K, Maier-Reimer, E. 2013. Global warming amplified

by reduced sulphur fluxes as a result of ocean acidification. *Nature Climate Change* **3**(11): 975–978. DOI: http://dx.doi.org/10.1038/nclimate1981.

Slezak, D, Kiene, RP, Toole, DA, Simó, R, Kieber, DJ. 2007. Effects of solar radiation on the fate of dissolved DMSP and conversion to DMS in seawater. *Aquatic Sciences* **69**(3): 377–393. DOI: http://dx.doi.org/10.1007/s00027-007-0896-z.

Smith, DC, Azam, F. 1992. A simple, economical method for measuring bacterial protein synthesis rates in seawater using 3H-leucine. *Marine Microbial Foodwebs* **6**(2): 107–114.

Spreen, G, Kaleschke, L, Heygster, G. 2008. Sea ice remote sensing using AMSR-E 89-GHz channels. *Journal of Geophysical Research: Oceans* **113**(C2). DOI: http://dx.doi.org/10.1029/2005JC003384.

Stefels, J, Steinke, M, Turner, SM, Malin, G, Belviso, S. 2007. Environmental constraints on the production and removal of the climatically active gas dimethylsulphide (DMS) and implications for ecosystem modelling. *Biogeochemistry* **83**: 245–275. DOI: http://dx.doi.org/10.1007/978-1-4020-6214-8_18.

Steiner, PA, Sintes, E, Simó, R, De Corte, D, Pfannkuchen, DM, Ivančić, I, Najdek, M, Herndl, GJ. 2019. Seasonal dynamics of marine snow-associated and free-living demethylating bacterial communities in the coastal northern Adriatic Sea. *Environmental Microbiology Reports* **11**(5): 699–707. DOI: http://dx.doi.org/10.1111/1758-2229.12783.

Stoecker, DK, Hansen, PJ, Caron, DA, Mitra, A. 2017. Mixotrophy in the marine plankton. *Annual Review of Marine Science* **9***:* 311–335. DOI: http://dx.doi.org/10.1146/annurev-marine-010816-060617.

Strong, C. 2012. Atmospheric influence on Arctic marginal ice zone position and width in the Atlantic sector, February–April 1979–2010. *Climate Dynamics* **39**(12): 3091–3102. DOI: http://dx.doi.org/10.1007/s00382-012-1356-6.

Strong, C, Rigor, IG. 2013. Arctic marginal ice zone trending wider in summer and narrower in winter. *Geophysical Research Letters* **40**(18): 4864–4868. DOI: http://dx.doi.org/10.1002/grl.50928.

Sunda, W, Kieber, DJ, Kiene, RP, Huntsman, S. 2002. An antioxidant function for DMSP and DMS in marine algae. *Nature* **418**(6895): 317–320. DOI: http://dx.doi.org/10.1038/nature00851.

Sunda, WG, Hardison, R, Kiene, RP, Bucciarelli, E, Harada, H. 2007. The effect of nitrogen limitation on cellular DMSP and DMS release in marine phytoplankton: Climate feedback implications. *Aquatic Sciences* **69**(3): 341–351. DOI: http://dx.doi.org/10.1007/s00027-007-0887-0.

Tang, CCL, Ross, CK, Yao, T, Petrie, B, DeTracey, BM, Dunlap, E. 2004. The circulation, water masses and sea-ice of Baffin Bay. *Progress in Oceanography* **63**(4): 183–228. DOI: http://dx.doi.org/10.1016/j.pocean.2004.09.005.

Teeling, H, Fuchs, BM, Becher, D, Klockow, C, Gardebrecht, A, Bennke, CM, Kassabgy, M, Huang, S, Mann, AJ, Waldmann, J, Weber, M. 2012. Substrate-controlled succession of marine bacterioplankton populations induced by a phytoplankton bloom. *Science* **336**(6081): 608–611. DOI: http://dx.doi.org/10.1126/science.1218344.

Thackeray, CW, Hall, A. 2019. An emergent constraint on future Arctic sea-ice albedo feedback. *Nature Climate Change* **9**: 972–978. DOI: http://dx.doi.org/10.1038/s41558-019-0619-1.

Theseira, AM, Nielsen, DA, Petrou, K. 2020. Uptake of dimethylsulphoniopropionate (DMSP) reduces free reactive oxygen species (ROS) during late exponential growth in the diatom *Thalassiosira weissflogii* grown under three salinities. *Marine Biology* **167**(9): 1–7. DOI: http://dx.doi.org/10.1007/s00227-020-03744-4.

Toole, DA, Siegel, DA. 2004. Light-driven cycling of dimethylsulfide (DMS) in the Sargasso Sea: Closing the loop. *Geophysical Research Letters* **31**(9): 5–8. DOI: http://dx.doi.org/10.1029/2004GL019581.

Toole, DA, Slezak, D, Kiene, RP, Kieber, DJ, Siegel, DA. 2006. Effects of solar radiation on dimethylsulfide cycling in the western Atlantic Ocean. *Deep Sea Res Part I: Oceanographic Research Papers* **53**(1): 136–153. DOI: http://dx.doi.org/10.1016/j.dsr.2005.09.003.

Trudnowska, E, Lacour, L, Ardyna, M, Rogge, A, Irisson, JO, Waite, AM, Babin, M, Stemmann, L. 2021. Marine snow morphology illuminates the evolution of phytoplankton blooms and determines their subsequent vertical export. *Nature Communications* **12**: 2816. DOI: http://dx.doi.org/10.1038/s41467-021-22994-4.

Uhlig, C, Damm, E, Peeken, I, Krumpen T, Rabe, B, Korhonen, M, Ludwichowski, K-U. 2019. Sea ice and water mass influence dimethylsulfide concentrations in the central Arctic Ocean. *Frontiers of Earth Science* **7**: 1–15. DOI: http://dx.doi.org/10.3389/feart.2019.00179.

Vance, T, Davidson, A, Thomson, P, Levasseur, M, Lizotte, M, Curran, M, Jones, G. 2013. Rapid DMSP production by an Antarctic phytoplankton community exposed to natural surface irradiances in late spring. *Aquatic Microbial Ecology* **71**(2): 117–129. DOI: http://dx.doi.org/10.3354/ame01670.

Varaljay, VA, Robidart, J, Preston, CM, Gifford, SM, Durham, BP, Burns, AS, Ryan, JP, Marin, III R, Kiene, RP, Zehr, JP, Scholin, CA. 2015 Feb 20. Single-taxon field measurements of bacterial gene regulation controlling DMSP fate. *ISME Journal* **9**: 1677–1686. DOI: http://dx.doi.org/10.1038/ismej.2015.23.

Veres, PR, Andrew Neuman, J, Bertram, TH, Assaf, E, Wolfe, GM, Williamson, CJ, Weinzierl, B, Tilmes, S, Thompson, CR, Thames, AB, Schroder, JC, Saiz-Lopez, A, Rollins, AW, Roberts, JM, Price, D, Peischl, J, Nault, BA, Møller, KH, Miller, DO, Meinardi, S, Li, Q, Lamarque, J-F, Kupc, A, Kjaergaard, HG, Kinnison, D, Jimenez, JL, Jernigan, CM, Hornbrook, RS, Hills, A, Dollner, M, Day, DA, Cuevas, CA, Campuzano-Jost, P, Burkholder,

J, Bui, TP, Brune, WH, Brown, SS, Brock, CA, Bourgeois, I, Blake, DR, Apel, EC, Ryerson, TB. 2020. Global airborne sampling reveals a previously unobserved dimethyl sulfide oxidation mechanism in the marine atmosphere. *Proceedings of the National Academy of Sciences U S A* **117**(9): 4505–4510. DOI: http://dx.doi.org/10.1073/pnas.1919344117.

Verity, PG, Brussaard, CP, Nejstgaard, JC, Van Leeuwe, MA, Lancelot, C, Medlin, LK. 2007. Current understanding of *Phaeocystis* ecology and biogeochemistry, and perspectives for future research. *Biogeochemistry* **83**(1–3): 311–330. DOI: http://dx.doi.org/10.1007/s10533-007-9090-6.

Vila-Costa, M, del Valle, DA, González, JM, Slezak, D, Kiene, RP, Sánchez, O, Simó, R. 2006. Phylogenetic identification and metabolism of marine dimethylsulfide-consuming bacteria. *Environmental Microbiology* **8**(12): 2189–2200. DOI: http://dx.doi.org/10.1111/j.1462-2920.2006.01102.x.

Wang, S, Elliott, S, Maltrud, M, Cameron-Smith, P. 2015. Influence of explicit *Phaeocystis* parameterizations on the global distribution of marine dimethyl sulfide. *Journal Of Geophysical Research Biogeosciences* **120**(11): 2158–2177. DOI: http://dx.doi.org/10.1002/2015JG003017.

Wassmann, P, Ratkova, T, Reigstad, M. 2005. The contribution of single and colonial cells of *Phaeocystis pouchetii* to spring and summer blooms in the north-eastern North Atlantic. *Harmful Algae* **4**(5): 823–840. DOI: http://dx.doi.org/10.1016/j.hal.2004.12.009.

Wassmann, P, Reigstad, M. 2011. Future Arctic Ocean seasonal ice zones and implications for pelagic-benthic coupling. *Oceanography* **24**(3): 220–231. DOI: http://dx.doi.org/10.5670/oceanog.2011.74.

Webb, AL, van Leeuwe, MA, den Os, D, Venables, H, Stefels, J. 2019. Interannual and interseasonal variation in DMS flux from the West Antarctic Peninsula. *Scientific Reports* **9**: 2233. DOI: http://dx.doi.org/10.1038/s41598-019-38714-4.

Woolf, DK. 1997. Bubbles and their role in gas exchange, in Liss, P, Duce, RA eds., *The sea surface and global change*. Cambridge University Press: 173–206. DOI: http://dx.doi.org/10.1017/CBO9780511525025.007.

Woolf, DK. 2005. Parametrization of gas transfer velocities and sea-state-dependent wave breaking. *Tellus B* **57**(2): 87–94. DOI: http://dx.doi.org/10.1111/j.1600-0889.2005.00139.x.

Zapata, M, Jeffrey, SW, Wright, SW, Rodríguez, F, Garrido, JL, Clementson, L. 2004. Photosynthetic pigments in 37 species (65 strains) of Haptophyta: Implications for oceanography and chemotaxonomy. *Marine Ecology Progress Series* **270**: 83–102. DOI: http://dx.doi.org/10.3354/meps270083.

Zeng, Y-X, Qiao, Z-Y, Yu, Y, Li, H-R, Luo, W. 2016. Diversity of bacterial dimethylsulfoniopropionate degradation genes in surface seawater of Arctic Kongsfjorden. *Scientific Reports* **6**: 33031. DOI: http://dx.doi.org/10.1038/srep33031.

How to cite this article: Galí, M, Lizotte, M, Kieber, DJ, Randelhoff, A, Hussherr, R, Xue, L, Dinasquet, J, Babin, M, Rehm, E, Levasseur, M. 2021. DMS emissions from the Arctic marginal ice zone. *Elementa: Science of the Anthropocene* 9(1). DOI: https://doi.org/10.1525/elementa.2020.00113

Domain Editor-in-Chief: Jody W. Deming, University of Washington, Seattle, WA, USA

Associate Editor: Jeff S. Bowman, Scripps Institution of Oceanography, UC San Diego, CA, USA

Knowledge Domain: Ocean Science

Part of an Elementa Special Feature: Green Edge

Published: July 14, 2021 **Accepted:** May 27, 2021 **Submitted:** August 7, 2020